GEOTHERMAL HEAT FLUX FROM HYDROTHERMAL PLUMES ON THE JUAN DE FUCA RIDGE

by

Karen G. Bemis

B. A., Geophysics, Rice University (1988)

Submitted to the
Massachusetts Insitute of Technology/
Woods Hole Oceanographic Institution
Joint Program in Oceanography and Oceanographic Engineering
in Partial Fulfillment of the Requirements
of the degree of

Master of Science

at the

Massachusetts Insitute of Technology
and the
Woods Hole Oceanographic Institution

May 1990

Signiture of Author_____
Joint Program in Oceanography and Oceanographic Engineering
Massachusetts Insitute of Technology/
Woods Hole Oceanographic Institution

Certified by_____
Richard P. Von Herzen
Senior Scientist, W.H.O.I.

Accepted by_____
George P. Lohmann, Chairman
Joint Committee for Marine Geology and Geophysics

GEOTHERMAL HEAT FLUX FROM HYDROTHERMAL PLUMES ON THE JUAN DE FUCA RIDGE

by

Karen G. Bemis

Submitted to the Massachusetts Insitute of Technology/ Woods Hole Oceanographic Institution Joint Program in Oceanography and Oceanographic Engineering on May 10, 1990 in partial fulfillment of the requirements of the Degree of Master of Science in Oceanography

Abstract

Estimates of the heat output of hydrothermal vents, identified along the Endeavor and Southern Segments of the Juan de Fuca Ridge, are used to evaluate the total heat flux associated with hydrothermal circulation for the ridge segment. An array carried by D/V ALVIN sampled the temperature and velocity structure of hydrothermal plumes from individual vents. The maximum heat flux calculated for a single vent is 50 MW, but the average vent output is only 13 MW per vent for 31 vents. The estimates for any given vent may vary over an order of magnitude. This uncertainty is due mainly to the difficulty of locating the centerline of the plume relative to the point of measurement, although the uncertainty in determining the constants from the appropriate equations based on laboratory experiments contributes a significant share to the net error. For the Endeavor Segment, the minimum total geothermal heat flux due to hydrothermal circulation exceeds 70 MW. The minimum estimate for the Southern Segment is 16 MW. The maximum estimate is probably closer to the total heat flux (236 MW and 66 MW respectively). The estimated heat flux density is 3300 W/m^2 for the Endeavor vent field and 39 W/m^2 for the Southern vent field. Focused hydrothermal venting accounts for only a small fraction of the heat available according to steady-state predictions of conductive heat flux; however, other hydrothermal phenomena (e.g., diffuse flow) account for the greater share of the total hydrothermal heat flux.

Thesis Supervisor: Richard P. Von Herzen
Title: Senior Scientist

Acknowledgements

I wish to thank Dick Von Herzen (my advisor), Debbie Smith, Jack Whitehead, Marcia McNutt, and Kathy Gillis for their good advice and unfailing support as I wrote my thesis and looked to the future. I have enjoyed my time at Woods Hole Oceanographic Institution. The navigation data used in my thesis was graciously processed by Vee Ann Atnipp and others in John Delaney and Russ McDuff's groups at University of Washington. Jerry Dean was not only extremely helpful on the cruise, but kindly answered my many questions afterwards. J. S. Turner supplied useful advice during his brief stay in Woods Hole. Both Chris Bradley and Andy Trivett have supplied helpful criticism and interesting commentary throughout the project. Additionally, I extend my thanks to the Atlantis II and ALVIN crews for their assistance on my 1988 cruise. This project was supported by NSF grant #OCE87-14511 and by the WHOI Education Office.

Table of Contents

List of Figures

List of Tables

Introduction

One-dimensional conductive cooling models of oceanic crust [Parsons and Sclater, 1977; Parker and Oldenburg, 1973; Davis and Lister, 1974] have been very successful in matching bathymetric and heat flow observations except in the near-ridge enviornment. The measured conductive heat flow near most ridge crests is less than that predicted by any conductive cooling model [Parker and Oldenburg, 1973; Davis and Lister, 1974; Parsons and Sclater, 1977]. This heat flow anomaly, defined by the difference between the measured and predicted conductive heat flow for a given model, is about 0.127 MW per meter ridge for the East Pacific Rise (EPR) and about 0.056 MW per meter ridge for the Mid-Atlantic ridge (MAR) [Sleep and Wolery, 1978; Morton and Sleep, 1985]. Sleep and Wolery [1978] among others have suggested that the heat flux associated with hydrothermal circulation is equal to the missing heat (the heat flow anomaly) at ridge crests. Various models have tried to quantify the effect of hydrothermal circulation on the conductive heat flow regime [Sleep and Wolery, 1978; Morton and Sleep, 1985; Green et al., 1981].

An independent determination of the magnitude of heat transfer by hydrothermal circulation would allow a quantitative assessment of models of the thermal and dynamic structure of ridge crests. Since hydrothermal circulation transfers heat from the base of the crust to the seafloor, I can use a measure of the heat output of the circulation system to estimate the overall heat transfer [Cann and Strens, 1985; Mottl, 1983]. Hydrothermal circulation in the crust has a range of manifestations [Gillis and

Robinson, 1988; Alt et al., 1986; Sleep, 1983]. At mid-ocean ridges, circulating seawater heats at depth and returns high temperature fluids directly to the seafloor (black smokers) or mixes with cold seawater or cools conductively resulting in low temperature fluids that exit at the seafloor (diffuse flow). Off-axis, cold seawater circulates through the seafloor with no detectable heat output. Only at the ridge does hydrothermal circulation transfer heat through the crust significantly faster than conductive cooling. As black smokers and diffuse flow are different surface expressions of the same circulation cell [Little et al., 1987], the relative heat transfer of each probably varies over location and time.

In my thesis, I present the results of a field program which concentrated on measuring the focused high temperature outflow from vents along the Juan de Fuca Ridge. An accurate estimate of the total heat transported from the crust by hydrothermal circulation must consider all heat-transport phenomena. These new data will complement the ongoing efforts to estimate the diffuse flow [A. Schultz, 1990; A. Trivett, personal communication] and the total hydrothermal heat flux [Baker and Massoth, 1987].

Geologic Setting

In the last several decades many geological and geophysical surveys have investigated the processes of crustal accretion along the Juan de Fuca Ridge; its rich history of dueling propagators and overlapping spreading centers has recently been recognized [e.g., Karsten et al., 1986; Kappel and Normark, 1987]. Overall, the Juan de Fuca Ridge is an intermediate-rate (30 mm/yr) spreading center in

the northeast Pacific. Hydrothermal vent fields have been described on several segments of the Juan de Fuca Ridge. This paper concentrates on the hydrothermal activity on the Southern Segment and the Endeavor Segment (Figure 1). A segment is a geologically and geophysically coherent length of ridge that may be defined as lying between significant ridge offsets (e.g. ridge transforms, overlapping spreading center) [Schouten et al., 1985]. The Endeavor and Southern Segments differ considerably in their present geology and active hydrothermal output.

The Endeavor Segment comprises a crestal ridge (4 km wide, 2100 m at its shallowest) that deepens to a broad valley (10 km wide, 3000 m at its deepest) towards each of the bounding overlapping spreading centers (Cobb offset to the south and Endeavor offset to the north) [Karsten et al., 1986]. A narrow (1-2 km), shallow (10-30 m) cleft extends along the ridge axis - normal faults form the walls of this inner rift [Karsten, et al., 1986]. Fissuring is apparent throughout the axial valley. Volcanism is most recently active in the inner rift, and pillow lavas dominate the volcanic features in the Endeavor Segment [Karsten et al., 1986]. Most, if not all, active hydrothermal vents have been found within the inner rift along the normal faults at the base of the western wall [Tivey and Delaney, 1986; Delaney et al., 1991].

In contrast to the Endeavor Segment, the Southern Segment comprises a relatively narrow axial valley (3 km wide) apparently formed as a collapse feature within a volcanically constructed crestal ridge [Kappel and Normark, 1987]. A very narrow (40-50 m), shallow (25-30 m) cleft, or inner rift, extends along the axis of the

valley [Kappel and Normark, 1987]. In the southernmost 20 km of the segment, the axial valley is floored by a lava plain broken only by the overlapping strands of the inner rift. Lava drain-back features suggest the inner rift may have been the site of fissure eruptions [Kappel and Normark, 1987]. North of the lava plain fissuring dominates the axial valley, although constructional volcanic cones are found near the lava plain. Sheet flows comprise the volcanics on the lava plain, but pillow lavas are found on the crestal ridges and flanks. Active hydrothermal venting occurs at several discrete locations along the inner rift whereas ubiquitously distributed sulfide deposits suggest either active hydrothermal venting along a greater length of ridge or changes in the locale of active venting in the past.

Besides the difference in distribution of hydrothermal sediments along the Southern Segment and the Endeavor Segment, each of these ridge segments has a distinct style of active hydrothermal venting. On the Endeavor Segment, large sulfide structures reaching 30 m in height extend up to 30 m along and 15 m across the strike of fissures. In contrast, the Southern Segment sulfide structures are simpler chimneys or spires (with major structures reaching 2 m in width) that only rarely reach 10 m in height [Tivey and Delaney, 1986; Shanks and Seyfried, 1987]. Although it is shorter in length, more active vent sites have been discovered along the Southern Segment (70 km) than along the Endeavor Segment (110 km) [Kappel and Normark, 1987; Karsten et al., 1986]. At the end of this paper, however, I show that the total heat flux is much lower for the Southern Segment vent fields.

Previous Estimates of Thermal Output

Previous attempts to measure the hydrothermal heat flux along the Juan de Fuca Ridge have yielded a broad range of estimates based on a variety of phenomena and assumptions. Baker and Massoth [1987] used CTD deep tows and water sampling to map the distribution of temperature, velocity, and light attenuation anomalies in a dispersing plume above the Endeavor Segment vent field. Plumes from individual vents reach a maximum rise height where they spread and coalesce to form a diffuse, but laterally extensive, cloud of temperature, particulate, and chemical anomalies. Based on the advective transport across a section of the plume as it drifted west, Baker and Massoth [1987] estimated the total heat flux at 1700 ± 1100 MW for two ~1 km^2 cross-sections 10 km apart on the Endeavor Segment. Similarly, they estimated a total heat flux of 580 ± 351 MW for two cross-sections upstream and downstream of the vent field on the Southern Segment. Crane et al. [1985] made a hydrographic survey along the axial valley of the segment. Using a line source model, they estimated a total heat flux of 1133 MW for 10 km of the Endeavor Segment. For the same data, they found a total heat flux of 1260 - 126,000 MW for advective flux through a vertical section along the ridge. The wide range of heat flux estimates is due to uncertainties in the estimates of current speeds. Similarly, for the Southern Segment the line source and advective flux models yield total heat fluxes of 2096 MW (for 40 km of ridge) and 3024 - 302,400 MW respectively.

Heat flux have also been estimated from chemical fluxes. Rosenburg et al. [1988] used radon as a tracer for plume emissions. The decay rate of radon was used to calculate the flux of radon into the plume: a radon/heat ratio calculated near the vent orifice was used to obtain a heat flux of 1000-5000 MW for the same vent field on the Endeavor Segment that I studied [Rosenburg et al., 1988].

Schultz et al. [1990] have recently estimated the diffuse heat flux out of an active sulfide "flange" on the Endeavor Segment to be around 1.4 MW/m^2 given measured effluent percolation velocities of 2-10 cm/s and temperatures of 7-13 °C. They also estimated the heat flux of a nearby high temperature vent to be 2.9 MW.

A point estimate of heat flux at a vent orifice can be made by multiplying the exit velocity, exit temperature, and areal cross-section of the vent orifice (knowing the heat capacity and density of the fluid). Macdonald [1983] estimated a heat flux of 60 ± 20 MW for a vent at 21°N on the EPR with 350°C water exiting at 2.5 m/s through a 0.08 m diameter exit. To demonstrate the inaccuracies of this method, Little et al. [1987] made a point estimate of heat flux higher in a hydrothermal plume at 11°N on the EPR. From a point estimate the calculated heat flux ranged from 0.04 to 0.59 MW compared to estimates of 2-4 MW based on the same data set using a theory relating the variation of temperature and velocity with height to heat flux [Little et al., 1987] (see below).

In 1984, Little et al. [1987] used an array similar to that described below for this study to measure the heat flux of black smokers at 11°N on the EPR. D/V ALVIN was stopped at several stations for 5-30 minutes to obtain profiles of the temperature

anomalies in the plumes. Little et al. [1987] used two different methods to calculate the heat flux based on the temperature anomalies. Based on the simple plume model (presented below) they obtained a heat flux estimate of 3.40 MW for a single vent or set of vents. Using a model accounting for the nonlinear dependence of seawater properties on temperature, they obtained a heat flux estimate of 2.76 MW. The simple plume model estimate is within 20% of the nonlinear plume model estimate.

Plume Behavior

To interpret the temperature and velocity data series, it is necessary to consider theoretical descriptions of plumes. An upwardly expanding plume is generated by a source of buoyancy and has no initial momentum [Little et al., 1987; Fischer et al., 1979]. A hydrothermal plume is actually a buoyant jet; that is, it has an initial source of both buoyancy and momentum. However, the effect of the initial momentum dies away rapidly with distance from the source. Beyond some critical distance, l_m, a buoyant jet behaves (and is) exactly like a plume [Fischer et al., 1979; Turner, 1973; Chen and Rodi, 1980]. In the following discussion I assume that the distance from the plume source (vent orifice) is sufficently large such that any intial momentum has completely decayed; this assumption is verified below. For a hydrothermal plume, the bouyancy source is generated by the temperature-dependent density contrast between the hot plume fluids and the cold ambient seawater.

Although a nonliner model, accounting for the temperature dependence of seawater properties, seems most appropriate for hydrothermal plumes, Little et al. [1987] demonstrated that, given the known inaccuracies in temperature and velocity measurements, the simple plume model is an adequate estimator of heat flux for hydrothermal plumes. Using the continuity equation and assuming a self-similarity law, Tennekes and Lumley [1972] show that plume behavior is governed only by the distance from the source of buoyancy. The velocity and temperature then depend only on the initial buoyancy flux, B_0 (in m^4/s^3) and the distance from the source, z (in m) (Figure 5). Note that buoyancy flux is assumed to remain constant with height, or increasing distance from the source. The following discussion follows the development in Fischer et al. [1979], but the values of the constants given are based on experimental results reported by Papanicolaou and List [1987]. Equations describing plume behavior are developed in terms of mean flow properties, where the means are averages over time and either averaged over space or at the plume centerline (Figure 5). The plume is assumed to rise vertically indefinitely within a homogeneous and current-free environment. The mean centerline velocity, W_c, is given by

$$W_c = b_1(B_0/z)^{1/3}, \qquad (1)$$

where b_1 is determined experimentally to be 3.85. Similarly,

$$T_c = b_4\ (B_0^2/z^5)^{1/3}/a/g, \qquad (2)$$

where T_c is the mean centerline temperature anomaly (excess over ambient water temperature), a is the coefficient of thermal expansion for seawater (1.48 x 10^{-4} 1/°C), g is the gravitational acceleration, and b_4 is determined experimentally to be 14.29.

If the plume is considered to emanate from a virtual point source of buoyancy at a distance z_0 from the vent orifice, where the momentum and volume fluxes go to zero, the initial momentum flux (at z = 0 m) is defined as

$$M_0 = b_2 (B_0^2 z_0^4)^{1/3}, \qquad (3)$$

where M_0 has dimensions of m^4/s^2 and b_2 is determined experimentally to be 0.290. To determine M_0, z_0 is calculated by assuming an initial (or exit) temperature, T_0:

$$z_0 = (b_4 B_0^{2/3}/a/g/T_0)^{3/5}. \qquad (4)$$

I redefine the mean centerline temperature in terms of the virtual height z_0 (or distance between the vent orifice and the virtual source) and the array height z (or distance between the vent orifice and the temperature reading):

$$T_c = b_4 (B_0^2/(z_0 + z)^5)^{1/3}/a/g, \qquad (5)$$

The distance l_m, beyond which the effect of the initial momentum flux is negligible, is defined as the distance where the buoyancy flux dominates the momentum flux.

$$l_m = M_0^{3/4}/B_0^{1/2} = b_2^{3/4}z_0. \qquad (6)$$

z_0 and l_m are the basic length scales governing plume behavior.

In my calculations of the observed heat fluxes at a vent, rather than using a simple substitution, I simultaneously fit the buoyancy flux and the virtual height. Starting with an initial virtual height of zero, the buoyancy flux B_0 and height $z_0 + z$ were repeatedly calculated in an iterative fashion using equations (4) and (5) until the virtual height z_0 remained constant between iterations. The heat flux was then calculated from the buoyancy flux.

Results

Field Program and Data Collection

I sampled 30 or more plumes associated with hydrothermal vents located along the Endeavor and Southern segments of the Juan de Fuca Ridge using a vertical instrumentation array, similar to that used by Little et al. [1987], attached to the submersible D/V ALVIN. The array, which is maintained vertically above ALVIN with flotation, carried five thermistors spaced at 10 m intervals above the basket on the front of ALVIN, where the array was attached (Figure 3). The temperatures measured by the thermistors have an instrumental resolution of 0.001°C, but electrical interference from D/V ALVIN's circuitry resulted in a practical resolution of about 0.05°C. At a height of about 22 m above the basket, just above the second thermistor, a combined flowmeter-CTD was attached. The flowmeter measured vertical and horizontal velocities in the range .01 - .20 m/s; 0.005 m/s is the stall-out speed [Weller et al., 1985]. To sample a given vent, the basket of ALVIN was driven as close to the vent orifice as considered safe (with care taken to avoid direct contact with the 350°C exiting fluids). The array extended upwards into the expanding plume.

Temperature and velocity were sampled every 2 and 14 seconds (with a response time of 2-3 seconds and an averaging time of 14 seconds respectively) respectively throughout each of 10 dives. Each dive data record was processed to yield five temperature profiles and one vertical velocity profile (Figure 4). Other useful variables were recorded by the flowmeter (pressure,

conductivity, horizontal velocity, tilt) and D/V ALVIN (pressure, transmissometry, altitude, location).

An attempt was made to sample all known vents in a limited area (Figure 2). Of ten dives made with the array, four (2112-2115) were at 47°57′ N along the Endeavor Ridge (Figure 2a); an additional dive (2116) was further north on the Endeavor Segment at 47°58' N (Figure 2b). The five remaining dives were spaced along the Southern Segment (Figure 2c): one (2119) at 44°41' N; two (2117,2121) at 44°40' N; and two (2118,2120) at 44°38' N. These locations on the Southern Segment correspond respectively with vent site 1, vent site 2 and the megaplume site reported in the literature [Kappel and Normark,1987].

The locations of the vents and the array data were determined using ship and in-hull navigation for D/V ALVIN. The in-hull navigation data consisted of travel times to 1 to 3 transponders of known location. Positions were determined geometrically using an uniform acoustic velocity of 1490 m/s with typical accuracies of ±1.5 m [Delaney et al., 1991]. Where the transponder geometry was less favorable, or distances too large for reliable round trip acoustic paths between ALVIN and the transponders, (as for the Southern Segment) inclusion of the surface ship as part of the acoustic network gave typical accuracies of ±10 m.

To simplify the analysis, I consider further only those sections (times) of the profiles when ALVIN was known to be stationary (generally, sampling a vent). ALVIN's motion, or lack of motion, was determined using the navigation records and verified by analysis of the dive video tapes and logs. The main advantage of this selection

criterion is knowing that the lower end of the array is fixed at a point close to the seafloor. This makes it possible to assume that each data string is a time series at a fixed point in space. However, the array is free to tilt away from the vertical with the attachment point as a pivot. The amount of tilt for a given current can be calculated by assuming the array consists of a massless string attached at the base to the seafloor (ALVIN stationary) with two cylinders of buoyancy attached at ~35 m (4-ball float) and ~55 m (3-ball float). I balanced the net buoyancy of the array (approximately 300 N and 600 N for the 4-ball and 3-ball floats respectively) and the force on the array from a horizontal current with the tension in the array to obtain a relationship between the net buoyancy and the horizontal current. I determined the force of the horizontal current from the viscous drag by assuming simple geometrical shapes for the floats [Gerhart and Gross, 1985]. A horizontal current of about 0.3 m/s could tilt the array by 10° from the vertical. Since 0.3 m/s is greater than observed current speeds on the Juan de Fuca Ridge [Thomson et al., 1989; Cannon and Pashinski, 1990; Cannon et al., 1991], large tilts (>10°) are unlikely. This is verified by the tiltmeters on the flowmeter which only rarely record tilts over 10° - and usually only when ALVIN is moving.

Results from Vent 2113-E

To illustrate the nature of the data set used for my heat flux calculations and to provide some of the results of those calculations, before going into the details of those the calculations, I have used vent 2113-E as a typical example of a vent measurement

(Figure 6). It is located near the middle of the Endeavor Segment vent field at transponder co-ordinates (4965, 6147). Figures 6-8 illustrate the data collected at vent 2113-E and the calculations discussed below. In summary, my calculations yeild a maximum and minimum heat flux of 24.6 MW and 8.2 MW, respectively, based on the temperature data from vent 2113-E. The velocity data are used to evaluate a separate estimate for the heat flux. For vent 2113-E, the velocity data yields a minimum and maximum heat flux of 2.7 MW and 35.3 MW, respectively.

For vent 2113-E and the heat flux estimates given above, the virtual height z_0 is estimated at 1.1 m assuming a vent exit temperature of 350°C. Based on this z_0, the length scale l_m is 0.4 m. For this vent, it is valid to neglect the effect of initial momentum beyond 0.4 m from the orifice. This validates the assumption of negligible initial momentum made in the development of equations (1) to (5).

Heat Flux Calculations

Using the above theory and experimentally determined constants, I wish to calculate the heat flux from the actual observed quantities. However, the theory is expressed in terms of centerline means and my observed data is a time series at some unknown distance from the centerline. Before I can calculate the desired quantities ($H=f\{B_0, z_0, l_m\}$), I need to estimate the centerline means, T_c and W_c, from the data.

A time series can be characterized in many ways. Two of the simplest measures are the maximum value and the sample mean.

Table 5 summarizes the data measures of temperature and velocity for each vent. The maximum value is easily found for any given set of observations assumed to be in a plume. I can relate the maximum observed value to the mean centerline value by comparing my data with laboratory experimental data (Figure 9). I note that, in general, the ratio C_{max}/C_c is constant with height and buoyancy flux (Table 4) where C is a given plume tracer (e.g. temperature, velocity).

The sample mean is also easy to determine, but the interpretation is more complicated because of the nature of plumes. A plume entrains, or engulfs, coherent volumes of the surrounding ambient fluid. These may be large and remain intact, even at the centerline, for some time period long with respect to the turbulent fluctuations [Papanicolaou and List, 1987]. If such a volume is advected past the array, the array appears to register ambient conditions, not plume conditions. If the array (or actually the individual thermistor) is known to be exactly stationary, this presents no problem. The theory given above, which is based on mean flow properties, already incorporates the effects of entrainment [Fischer et al., 1979; Tennekes and Lumley, 1972; Papanicolaou and List, 1987]. However, if the position of the array is unsteady (due to fluctuations in the position of the plume or to ambient flow patterns), the sample mean would incorporate true ambient conditions as well as plume and apparent ambient conditions and thus underestimate the desired mean. Unfortunately, a fixed point time series is unverifiable for an array with only vertically offset thermistors. Horizontal control is desirable and a subject for future experimentation. For this reason, the sample

mean is calculated in two different ways: first, assuming a fixed point and including all observations (indicated by the subscript cold; e.g. T_{cold}) and second, assuming that all apparent ambient conditions derive from measurements while the array element is located external to the plume boundaries and removing all such observations from the data string (indicated by the subscript hot; e.g. T_{hot}). To relate the observed sample means to mean centerline values, I note that an observed mean is a time average at some fixed, but unknown, radial distance r from the centerline. The centerline mean could be easily calculated if r were known, since from laboratory data I know that the time-averaged profile of a plume tracer is approximately Gaussian [Fischer et al., 1979; Papanicolaou and List, 1987]:

$$C(r) = C_c \exp(-(r/b)^2), \qquad (7)$$

where C(r,z,t) is the value of some tracer (e.g. temperature, velocity) at a particular location in time and space (r,z,t), C(r) is C(r,z,t) evaluated at a given z and averaged over the time t, C_c is C(0) for the same z and averaged over t, and b is the half-width of the plume at z. The ratio b/z is the expansion rate of a plume, a constant independent of buoyancy flux [Fischer et al., 1979; Papanicolaou and List, 1987]. Therefore, the centerline value is given by

$$C_c = C(r) \exp(r/b)^2. \qquad (8)$$

However, if r is unknown and cannot be deduced, I cannot solve for C_c. In the following I discuss how I dealt with this impasse and succeeded in at least bounding the heat output of each vent under study.

Temperature Measurements

Temperature in a thermally buoyant jet may seem to play an important dynamic role as the source of buoyancy, but it can easily be shown that temperature anomalies actually behave like a passive tracer [Fischer et al., 1979]. Most theories are developed in terms of tracer concentrations [e.g., Chen and Rodi, 1980; Papanicolaou and List, 1979; Fischer et al., 1979]. The following discussion [see discussion of jets in Fischer et al., 1979] is in terms of temperature. Note that the heat flux H depends only on the buoyancy flux B_0, the source term used below:

$$H = \frac{\rho c_p}{\alpha g} B_0 \qquad (9)$$

where ρ is the density of the plume fluid, c_p is the heat capacity, α is the coefficient of thermal expansion, and g is the gravitational acceleration.

Suppose the heat flux remains constant with distance from the source of the plume and equals the source supply rate of heat. This assumption holds for constant buoyancy flux and negligible diffusion rates. Define

$$\mu T_{av} = QT_o = H/pc_p = B_0/ag \qquad (10)$$

where μ is the volume flux, T_{av} is the flow-weighted average temperature, Q is the initial volume flux, T_o is the initial (or exit) temperature, and H is the supply rate of heat [Fischer et al., 1979]. Using this assumed property of a plume, I can infer the relationship between the flow-weighted average temperature T_{av} (which is a function of distance from the source) and the time-averaged mean centerline temperature T_c (also a function of distance from the source). In particular, both the volume flux and the mean centerline temperature can be written as functions of buoyancy flux, B_0, and distance from the source, z:

$$\mu = b_3 B_0^{1/3} z^{5/3}, \qquad (11)$$

$$T_c p c_p / H = b_4 B_0^{-1/3} z^{-5/3}, \qquad (12)$$

where b_3 and b_4 are dimensionless constants experimentally determined to be 0.140 and 14.29 respectively [Fischer et al., 1979; Papanicolaou and List, 1988]. By combining equations (10), (11) and (12), I obtain [Fischer, et. al, 1979]

$$T_c/T_{av} = b_3 b_4, \qquad (13)$$

which allows me to convert flow-weighted average temperatures to mean centerline temperatures.

My data, however, yields time-averaged temperatures at a given, but unknown, radial array distance r from the centerline. I note that the flow-weighted average temperature T_{av} as defined by equations (9) through (13) is equal to the time averaged temperature T(r) at some radial distance r=R (Figure 10). For a Gaussian profile, where

$$T(r)=T_{av}\exp(r^2/b_c^2), \qquad (14)$$

I can solve for R by substituting in $T_{av}=T_c/b_3b_4= 0.5T_c$ (from equation (13) and Table 3) for T(r). At $R=0.69b_c$ the time-averaged temperature is equal to the averaged flow-weighted temperature of a Gaussian plume. By assuming that my temperature anomalies were measured approximately at R, I can estimate the mean centerline temperature using equation (13) and hence the heat flux using equations (6) and (9).

An alternative is to develop a solution to the system of equations generated by evaluating equations (2) and (14) at two or more vertically spaced thermistors. The derivation of this solution is given in Appendix I. The theory of this approach is sound, because I assume only that temperature is measured at a constant radial distance from the centerline in addition to the assumptions implicit in the use of simple plume theory as presented above. However, in practice it appears to be unstable. If all five of my thermistors are used in pairs, the calculated radial distances deviate significantly from each other as do the calculated heat fluxes contradicting the assumptions of constant radial distance of the array from the

centerline and constant heat flux (or buoyancy flux) with increasing height (Table 7). This could be the effect of merging plumes or a plume bent over by a crossflow. Additionally, unusually high temperatures ratios result in an imaginary radial distance, which is physically unreasonable. (The temperature ratio is defined as the temperature measured by the lower thermistor divided by the temperature measured by the upper thermistor.) An higher-than-usual ratio probably results from the upper thermistor being farther from the plume centerline than the lower thermistor; an effect probably due to a crossflow bending over the plume. In conclusion, this approach appears more sensitive to the effects of a crossflow or merging plumes than the approach presented earlier in this paper. However, both this approach and the earlier approach yield the same range of heat flux estimates (Table 7) validating my use of the first method to calculate the heat fluxes reported in this paper.

The first method presented has two intrinsic sources of error. First, it assumes the array is at a given radial distance from the plume centerline ($R=0.69b_c$) while the actual radial distance is unknown. If my measurements are closer to the centerline, I will overestimate the heat flux. For comparison, I also evaluate the heat flux assuming a radial distance of zero (i.e. the array is at the centerline), which is then a minimum bound.

The second intrinsic source of error is the various dimensionless constants needed for a numerical evaluation. The parameter values used in the calculations are all calculated from the results reported in Papanicolaou and List [1988], a very thorough study, using modern techniques of measurement in fully developed

plumes. Most previous estimates of the parameters are based on measurements in the region of transition between jet-like to plume-like behavior. The differences in the parameter estimates appear small (Table 1). However, the estimates of heat flux H are sensitive to fairly small changes in the parameters -- the new parameters yield heat fluxes twice those using the old values.

Another method of calculating heat flux from my temperature measurements uses the maximum recorded temperature. Laboratory data presented in Papanicolaou and List [1987;1988] suggest that the maximum temperature is a constant multiple of the centerline temperature (Figure 9). The ratio of maximum to mean centerline temperature is 1.5 to 2.5 for plumes (See Table 4). However, there are insufficient data to know if the ratios based on data reported by Papanicolaou and List [1987] hold for all buoyancy fluxes and Reynolds numbers in plumes. The Reynolds number is a nondimensional parameter measuring the relative strength of inertial and viscous forces; it is defined as $Re = uD/v$, where u is the velocity, D the diameter, and v the dynamic viscosity. The Reynolds number provides some indication of the degree of turbulence present. For my data, the heat flux calculated from the maximum temperature generally lies between the bounds on heat flux given by the mean temperature. Since a centerline location is assumed, the maximum temperature ought to provide a minimum estimate of heat flux. However, because of uncertainties in the empirical basis of the conversion to a mean centerline temperature and in the general turbulent behavior of plumes, I do not place much reliance on such a minimum.

Figure 7 shows the various determinations of the mean centerline temperature discussed above plotted against height and compared with the theoretical relationship between temperature and height at a given buoyancy flux for the vent 2113-E. This plot illustrates clearly which thermistors were closest to the centerline. The thermistor closest to the centerline registers the highest estimates of heat flux (but not necessarily the highest temperatures); the high estimate based on the mean observed temperature and the high estimate based on the maximum observed temperature should both register on the same thermistor. In determining the range of possible heat fluxes, I assume the thermistor registering the highest heat flux is closest to the centerline (this should always be true) and use the data from that thermistor to determine the minimum and maximum estimates of heat flux for a given vent (Table 6).

Velocity Measurements

A relation can also be derived between the time-averaged velocity and the spatially-averaged velocity. However, because velocity is tied to the basic turbulent processes in an active rather than passive sense, the form of such a relationship can be expected to be more complicated than for temperature.

As for temperature, I define a spatially-averaged velocity as a function of volume flux. Volume flux in the simplest sense is average velocity times the area through which the fluid moves:

$$w_{av} = \mu/A = \mu/(\pi R^2), \qquad (15)$$

where w_{av} is the average velocity as defined above, μ is the volume flux, A is the cross-sectional area and R is the effective plume radius. The volume flux μ is (implicitly) integrated to include all velocities from the centerline to an infinite distance, but the area of the plume is (of necessity) defined as a finite portion of the plume. The excluded area includes a sufficient amount of integrated velocity to exactly compensate for the lowered velocities away from the centerline within the included area. So I must explicitly integrate for the volume flux to match the area of integration with the area of measurement. Thus I define w_{av} as

$$w_{av} = \frac{1}{A}\int_A w(r)dA = \frac{1}{2\pi b_w^2}\int_0^{\sqrt{2}\,b_w} w(r)2\pi r dr \qquad (16)$$

where A is the area of a horizontal cross-section of the plume, when a Gaussian profile with half-width b_w, the radial distance from the centerline where the velocity is 1/e of its centerline value,

$$w(r) = w_c \exp(-r^2/b_w{}^2). \qquad (17)$$

To include all the velocities in the integration out to the detection limit, we integrate out to the radial distance $\sqrt{2}\ b_w$, where velocity is $1/e^2$ of its centerline value. Upon integration, equation (16) yields

$$w_c/w_{av} = (1-1/e^2)/2 \approx 0.43. \qquad (18)$$

I could use this ratio to estimate the time-averaged mean centerline velocity from a spatial average of velocity measurements between r=0 and $r=\sqrt{2}b_w$. But, as for temperature, my data yields only time-averaged velocities at an unknown radial distance from the centerline. So again I assume the array is located at the radial distance R where the time-averaged velocity equals the spatially averaged velocity (Figure 11). Substituting w_{av} as given by equation (18) for w(r) in equation (17), I find that R is $0.92b_w$. As before, if my measurements are taken closer to the centerline, I will overestimate the heat flux. Calculation of the heat flux assuming R=0 yields a minimum bound.

Alternatively, I can estimate the heat flux from the maximum observed velocity. At the centerline, the maximum velocity is larger than the mean velocity by a factor of 1.65 for laboratory plumes [Papanicolaou and List, 1988]. This ratio is well established by various laboratory experiments (Figure 9) and should yield a reasonable minimum estimate for heat flux.

Measurement Errors

Besides the errors intrinsic to my assumptions and theory, there exist errors associated with the measurement process itself. One source of error is the uncertainty in constraining the distance above the source. Although the relative distance between thermistors is known to a tenth of a meter, the absolute height, or distance from the source, could be off by an unknown distance on the order of meters. This is a critical consideration when 1) ALVIN is in a region of multiple plumes or 2) ALVIN has parked above or below the exit of a chimney. Although both occurred, the video tapes and observer dive logs suggest the former was more common than the latter.

However, most of the uncertainty in the heat flux estimates probably comes from the uncertainty in the location of the centerline. Because of the intense entrainment of ambient fluid into plumes, it is impossible to determine anything about the location (relative or absolute) of the centerline from a measurement (e.g. temperature) record. A low flux, near centerline record could appear identical to a high flux, far centerline record. Spectral patterns or energy levels might allow me to differentiate between these cases, but the experimental (laboratory) data needed to constrain such determinations is still limited.

As the above shows, any estimate could be so inaccurate as to be meaningless. However, the maximum-temperature-based heat flux is expected to underestimate the true heat flux unless the array is very close to the centerline ($r \approx 0$). Additionally, the mean-temperature-based heat flux overestimates the true heat flux when

$r < 0.69b_c$. The actual heat flux should be within the bounds provided by my estimates.

One of the problems with using the velocity data is the buoyancy flux (and thus the heat flux) is proportional to the cubic power of the mean centerline velocity (equation (1)). Thus small uncertainties in velocity (on the order of ±0.005 m/s, the resolution of my data), result in large uncertainties in the heat flux (±2.5 MW for a heat flux near 15 MW; ±0.2 MW for a heat flux near 0.5 MW).

Since the distance from the source, or height, is linearly related to the buoyancy flux, a small error (± 1 m) in the height has a negligible effect on the calculated heat flux. A height of 21.4 m has been used for the velocity data. The flowmeter has a length of 2.1 m and the propellers measuring velocity are at both ends - so an error of up to 2 m is possible. However, increasing the height by 1 m raises the estimated minimum heat for vent 2113-E only by 0.1 MW from 2.7 MW to 2.8 MW. Clearly the accuracy of the velocity data itself is more important.

Other factors besides the limiting resolution affect the accuracy of the velocity data. Each propellor covers an area of about 25 cm^2 compared to the thermistors which sample an area less than 1 cm^2. A lower heat flux would be estimated for the larger area since the recorded velocity will be an average (not a maximum) of the velocities in that area. Additionally, the propellers extend about 0.5 m laterally from the array. This could decrease or increase the heat flux estimated from velocity relative to the heat flux estimates from temperature. Finally, the flowmeter is at 21.4 m, but the thermistor closest to the centerline was usually the fourth

thermistor (40.4 m) not the second thermistor (21.4 m). Generally, the velocity and temperature data yield similar estimates of heat flux. However, the velocity-based estimates do appear to be lower on average, but from the arguements above that may not be unexpected.

Environmental Factors

A final source of error concerns the basic assumptions of plume theory. Plume theory is derived assuming a surrounding environment that is homogeneous and stationary. In the real ocean, the water column is stably stratified and currents are common. At the Juan de Fuca Ridge, horizontal currents of up to 0.20 m/s have been observed although the mean current flow is generally 0.05 m/s [Thomson et al., 1989; Cannon and Pashinski, 1990]. The water column is also stratified [Baker and Massoth, 1987]. However, the bottom 50 to 100 m of the water column appear nearly homogeneous based on the temperature and conductivity data collected in this study. Stable stratification affects plumes mainly by limiting the rise height to the region of neutral buoyancy, at which point the plume spreads horizontally [Fischer et al., 1979]. Since the array is generally in the homogeneous region and the expected rise height is around 100 m, the error introduced into heat flux calculations is insignificant.

The effect of a current is more complicated to assess. For relatively short times (hours), a steady crossflow in the region of the plume can be assumed. The general effect is to bend over and break up the normal plume flow (Figure 12). The exact effect

depends on the relationship of the height of measurement, z, and a length scale, z_B, specifying the height at which the crossflow dominates the normal plume behavior. z_B is defined in terms of the buoyancy flux B_0 and the crossflow velocity U [Fischer et al., 1979]:

$$z_B = B_0/U^3. \tag{19}$$

If $z << z_B$, which can be shown almost always to be true for black smokers at heights less than 50 m, the plume behaves very close to that predicted by simple plume theory. The velocity has the same relation to height and buoyancy flux, although scaling factors (that cancel) are introduced.

$$w/U \approx (z/z_B)^{1/3} \tag{20}$$

[Fischer et al., 1979]. Equation (20) becomes

$$w \approx (B_0/z)^{1/3} \tag{21}$$

on substitution of the definition of z_B. The functional form of the temperature relation is unchanged although there may be a new constant factor introduced. The normalized tracer concentration $\emptyset(z)$ has the same z dependence.

$$(z_B/z_M)^2(gM_0\emptyset(z)/UB_0) = D(z_B/z)^{5/3} \tag{22}$$

[Fischer et al., 1979]. Equation (22) becomes

$$\emptyset(z) = D(B^4/z^5)^{1/3}/g \qquad (23)$$

on substitution of the definition of z_B (equation 19) and when D is a constant and z_M is $M^{1/2}/U$. For $z < 50$ m and $H > 0.1$ MW, an ambient current of 1 cm/s can be ignored. Currents of up to 50 cm/s have been observed on the Juan de Fuca Ridge [Thomson et al., 1989; Cannon and Pashinski, 1990]. Although horizontal velocities up to 30 cm/s were measured on several dives (uncorrected for ALVIN motion), in the immediate vicinity of a vent the average horizontal velocity was generally close to zero. For vent 2113-E, two perpendicular components of horizontal velocity are plotted against each other (Figure 13) -- the apparently random distribution in time and space of velocity vectors about zero argues that the mean horizontal velocity in this case is nearly zero. Generally, it seems reasonable to ignore the crossflow as a first approximation; the error introduced is probably small compared with that from other sources.

Recommedations for Future Experimental Design

Of the sources of error discussed above, those involving the spatial location of the measurements could be avoided or better resolved by changing the design of the measurement array. The error in locating the array relative to the plume centerline and orifice can be mitigated and resolved by a knowledge of the horizontal variations. Thermistors spaced symmetrically about the array on the order of b_w (the plume half-width) apart would measure the

horizontal variations in temperature giving an indication of the distance from the centerline. The error due to the uncertainty in the parameters will only be resolved by many careful laboratory experiments. The environmental factors can be accounted for by modifying the equations used, if desired.

Discussion

In spite of the significant uncertainties in each heat flux estimate, they yield some useful comparisons with theoretical predictions of geothermal heat flux and with previous estimates of the geothermal heat flux due to hydrothermal circulation (Figure 3). The minimum total heat flux observed on the Endeavor Segment is 70 MW (the sum of the individual minimum heat fluxes measured - Table 10). A maximum estimate of 236 MW is probably closer to the total heat flux from the sampled vents; the maximum estimate fits the expected results from a visual comparison of the data profiles. It also matches the results of alternative calculation methods closer than the minimum estimate does. Both numbers are much smaller than most of the heat flux estimates quoted in the introduction. Estimates based on measurements in the upper water column yield heat fluxes on the order of 10^3 - 10^4 MW for the full Endeavor Segment vent field -- a factor of 10 - 10^2 greater than my results. The total area covered by the vent field based on the mapped distribution of the sampled vents (Figures 2a and 2b) is approximately 0.07 km^2 (0.035 km^2 for dives 2112 to 2115 and 0.035 km^2 for dive 2116, which was significantly farther north). The average heat flux density (heat flux per unit area of seafloor) is 1000 to 3300 W/m^2.

The minimum total heat flux observed on the Southern Segment is 16 MW (the sum of the individual minimum heat fluxes). The maximum observed heat flux of 66 MW is probably closer to the true heat flux as explained above. As for the Endeavor Segment, both numbers are much smaller than most of the heat flux estimates

quoted in the introduction. Estimates based on measurements in the upper water column yield heat fluxes on the order of 10^3 - 10^4 MW for the combined Southern Segment vent fields -- a factor of 10 - 10^2 greater than my results. The total area covered by the vent field (Figure 2c) is approximately 1.69 km^2 (0.36 km^2 for dive 2119, 0.87 km^2 for dives 2117 and 2121, and 0.46 km^2 for dives 2118 and 2120). The average heat flux density (heat flux per unit area of seafloor) is 9.5 to 39 W/m^2.

The upper water column estimates may be biased by the temporal storage of heat in the (relatively narrow) inner rift valley of both segments of the Juan de Fuca Ridge [M.K. Tivey, personal communication]. Topography exerts a greater control on the dispersion of heat flux in the axial valley of the Southern Segment than on the axial ridge of the Endeavor Segment. Additionally, the advective flux is only as accurate as the mapping of temperature and velocity fields. Baker and Massoth [1987] based their estimates on mean currents and the asymmetric shape of the advected plume.

Estimates at a single vent orifice on the EPR yield ~60 MW [Macdonald et al., 1980; Macdonald, 1983; Converse et al., 1984] which are about a factor of 10 greater than my results, but such estimates have primarily been made for the highest temperature vents. The individual vents there vary by at least a factor of 10^2 in their heat output [Macdonald et al., 1980; Little et al., 1987]. Additionally, a careful determination of water properties near the critical point is essential for accurate point estimates under exit conditions [Macdonald et al., 1980].

On several of our dives (e.g., 2114-B thru D) ALVIN circled a sulfide structure and took array measurements at several stations (Tables 5-10). Generally, several black smokers were observed on the structure in these cases as well as shimmering water, flanges, and tubeworm patches. To avoid overestimating the total heat flux due to including the same plume twice, I only counted a vent sample as unique if it was more than one plume width (~10 m at a height of 50 m) distant from other vent samples.

Multiple sampling of the same edifice can indicate (1) how well I have sampled a given plume, (2) how much heat output varies for a given structure, and (3) the extent of plume merging at a given height. An analysis of how the estimates of heat flux correlate with spatial location suggests that measuring the plume temperatures at different distances from the plume centerline accounts for most of the variation in the heat flux estimates at a given sulfide structure. However, some variations can not be accounted for in this way. Plume merging appears to elevate the general level of heat transport at heights of 40 and 50 m in the vicinity of a multiple smoker edifice. Variations between stations at lower heights are more likely to be due to actual differences in smoker outputs. Some variation in the degree of mixing of hot hydrothermal fluids with cold seawater before exiting between chimneys on large sulfide edifices is inferred from differences in the exit temperatures and chimney structure. A reasonable explanation of how chimneys grow and die on a large sulfide structure is presented by Tivey and Delaney [1986].

On dive 2117 ALVIN circled a single black smoker stopping four times during its tour. The data from these four stations is reported as vent labels 2117-D, 2117-E, 2117-F, and 2117-G in Tables 5-7. The minimum heat flux estimates vary between 0.4 MW and 0.6 MW while the maximum heat fluxes vary between 2.0 MW and 2.3 MW. In both cases, the variation is smaller than the error (approximately ±0.5 MW) due to the resolution limitations in measuring temperature (±0.05 °C). The video record suggests the array was at a uniform distance of about 1 m from the plume. Although the navigation is not accurate enough to confirm that all measurements were taken at a similar distance, this suggests that the plume was rising vertically rather than bending to one direction (where higher temperatures would be measured) due to ambient currents. Thus my assumption of a vertically rising plume (in the development of simple plume theory) seems partially justified in this case.

The Southern Segment vent fields have a significantly lower heat output than the Endeavor Segment vent fields. This is corroborated by lower temperatures, less vigorous smoking, and smaller sulfide structures in the Southern Segment. It is surprising in that volcanic activity appears to have occurred more recently along the Southern Segment and present hydrothermal activity covers a larger portion of the Southern Segment ridge. Hydrothermal activity does not seem to always correlate well with the availability of an immediate heat source [Karsten et al., 1986; Kappel and Normark, 1987]. Recently, however, hydrothermal

activity has been observed in connection with a recent lava flow [Embley et al., 1990].

Geological Implications

A comparison with theoretical models of heat flux at spreading ridges suggest that hydrothermal circulation accounts for the "missing heat" observed at the ridge crest. The missing heat flow at the ridge crest suggests a maximum hydrothermal heat transport of 0.039 MW/m for the Juan de Fuca Ridge (value calculated using data from Moran and Lister [1987] as explained in Appendix II). Focused high temperature venting accounts for only 1-5% of the missing heat: for the Endeavor Ridge a missing heat flux of 4300 MW (110 km x 0.039 MW/m) compares with my observed hydrothermal heat flux for the Endeavor Segment of 70-236 MW. Similarly, for the 70 km Southern Segment my result of 16-70 MW compares to a missing heat of 2700 MW. Estimates of the total hydrothermal heat flux that include the diffuse flow (Table 2) account for most of the missing heat.

Morton and Sleep [1985] model the effect of hydrothermal circulation on the temperature structure at the ridge crest. They use point heat sinks to simulate the cooling effect of hydrothermal circulation and point heat sources to simulate the effect of conduction and latent heat from the magma chamber. By letting the number of heat sinks vary, the depth to the magma chamber was matched to data from seismic reflection studies. A seismic reflection study of the southern Juan de Fuca Ridge suggests that the roof of a magma chamber lies at a depth of 2.5 km [Morton,

1984]. A predicted maximum heat flow of 0.010 MW per meter ridge from hydrothermal circulation was determined for the southern Juan de Fuca Ridge - this accounts for about 10-20% of the missing heat, assuming that the Juan de Fuca Ridge has a similar difference between the observed and theoretical heat flow as do the EPR and the MAR. Morton and Sleep [1985] suggested that cooler circulation cells off ridge might account for the remaining 80-90% of the missing heat. Their result predicts 700 MW of missing heat for the Southern Segment (based on the above heat flux density of 0.010 MW per meter ridge) compared with the observed geothermal heat flux of 16-70 MW due to hydrothermal circulation on the Southern Segment (this study). Morton and Sleep's [1985] model may overestimate the hydrothermal heat flux. However, observations of hydrothermal heat flux that include diffuse flow and do not rely on locating individual vents yeild heat fluxes of 500-1000 MW for the Southern Segment. These values are commensurate with Morton and Sleep's [1985] results.

The heat source at mid-ocean ridges is the magma emplaced at shallow depth in the process of creating new crust. Three models of this process are considered below: (1) the crystalizing of a small magma chamber, (2) the cracking of hot rock, and (3) the cooling of a slab of new crust. Based on seismic reflection studies [Morton, 1984], any magma chamber under the ridge crest is less than 1-2 km wide. For simplicity I consider a 1 km^3 magma chamber (1 km^2 cross-section along 1 km of ridge) with a latent heat of crystallization of about 1028 MJ/m^3 for basalt [Morton and Sleep, 1985]. Therefore about 1 x 10^{12} MJ of heat are released in

crystalizing a 1 km^3 magma chamber. The heat flux depends on the length of time over which the magma chamber crystalizes; solidification generates 6 MW if the magma chamber crystalizes completely in 5000 years (crystallization time for a 1 km thick dike according to the model presented in Turcotte and Schubert [1982] using crustal parameters). The heat flux of 6 MW per 1 km^3 of magma can be considered as 6 MW per 1 km ridge for a continuous magma chamber with a 1 km^2 cross-section; the heat flux for a longer ridge length can be determined by multiplying by the total ridge length, assuming the 1 km^2 cross-section. Some of this heat could be conducted away. In comparison this study observed minimum hydrothermal heat fluxes of 70 MW and 16 MW for the Endeavor and Southern Segments respectively. A continuous magma chamber the length of either ridge segment could supply heat at these rates in a steady-state system. However, the length of the magma chamber must be consistent with seismic and other geophysical data.

According to Lister [1983; 1974], cold water can cool hot rock by progressive cracking. Different parameter values yield different flux rates for a propagating crack front. For the model presented by Lister [1983], bounds placed on the crack spacing and the boundary layer thickness limit the heat extraction rate to between 280 W/m^2 to 24000 W/m^2. This compares to the minimum calculated removal rates of 1000 W/m^2 and 9.5 W/m^2 for the Endeavor and Southern Segments.

New crust is created in proportion to the spreading rate (a half-spreading rate of 30 mm/yr is appropriate for the Juan de Fuca

Ridge). Assuming crustal accretion occurs evenly along a ridge segment, the new crust can be modeled as a injected slab the length of the ridge (Figure 14). The width is assumed to be proportional to the spreading rate($D = 9.52 \times 10^{-10}$ m/s). With an initial temperature T_0 of 1185°C, the amount of heat is given by

$$Q = pc_pLDz_D(T_0 - 0.5az_D), \qquad (24)$$

where z_D is the maximum depth of the slab (assumed to be the probable depth to any magma chamber, 2.5 km), a is the average thermal gradient for oceanic crust, pc_p is the specific heat per volume of basalt (2.95×10^6 J/m^3/°K), and L is the length of ridge. For these parameters, Q/L is 0.0081 MW per meter ridge. This is larger than the conductive cooling rate (0.0018 MW/m) calculated by Morton and Sleep [1985], but similar to the rate of hydrothermal cooling (.0084 MW/m) they calculated. I have calculated Q for the appropriate ridge lengths to get 900 MW for the Endeavor Segment (110 km) and 570 MW for the Southern Segment (70 km) as compared to the observed minimum hydrothermal heat flux of 70 MW and 16 MW, respectively.

Conclusions

I have calculated total heat fluxes of 70-236 MW for the Endeavor Segment and 16-66 MW for the Southern Segment vent fields from temperature and velocity profiles of hydrothermal vents observed with D/V ALVIN. I quantified the contribution of focused hydrothermal venting to the missing heat, or conductive heat flow

anomaly at the Juan de Fuca Ridge. My results are consistent with the conclusions of other investigators that hydrothermal circulation plays a important role in the cooling of newly accreted crust [Davis and Lister, 1974; Parsons and Sclater, 1977; Cann and Strens, 1982; Lister, 1983; Mottl, 1983]. The minimum observed hydrothermal heat flux along the Juan de Fuca Ridge from high temperature venting is less than the long-term rate of heat supply. However, estimates of the hydrothermal heat flux that include a broader range of phenomena match the long-term rates of heat supply predicted by any reasonable model of crustal accretion. Diffuse flow phenomena transport must heat a faster rate than black smokers.

Appendix I

Rewriting equation (16) to include the height dependence explicitly and substituting equation (2) for T_c yields

$$T = \frac{b_4}{ag}\left(\frac{B_o^2}{z^5}\right)^{1/3} e^{-(r^2/z^2)(z/b_c)^2} \qquad (25)$$

where b_c/z is a plume expansion constant determined by laboratory experiments to be 0.112. I produce a set of simultaneous equations by substituting the observed temperatures (T_1, T_2) at two different heights (z_1, z_2) into equation (25):

$$T_1 = \frac{b_4}{ag}\left(\frac{B_o^2}{z_1^5}\right)^{1/3} e^{-(r^2/z_1^2)(z/b_c)^2} \qquad (26)$$

$$T_2 = \frac{b_4}{ag}\left(\frac{B_o^2}{z_2^5}\right)^{1/3} e^{-(r^2/z_2^2)(z/b_c)^2} \qquad (27)$$

Assuming that the buoyancy flux B_o and the radial distance r of the array from the centerline are both constant with height z, I solve the equations (26) and (27) simultaneously to obtain

$$r = \left(\frac{\log\left(\frac{T_1}{T_2}\left(\frac{z_1}{z_2}\right)^{5/3}\right)}{\left(\frac{z}{b_c}\right)^2\left(\frac{1}{z_2^2} - \frac{1}{z_1^2}\right)}\right)^{1/2} \qquad (28)$$

$$B_o = \left(\frac{b_4}{ag}\right)^{-3/2}\left(\frac{T_2^{\Omega}}{T_1}\right)^{3n/2}\left(\frac{z_2^{\Omega}}{z_1}\right)^{5n/2} \qquad (29)$$

where $\Omega=(z_2/z_1)^2$ and $n=1/(\Omega-1)$. Equations (28) and (29) are independently derived and either could be used in combination with equations (2) and (14) to evaluate all of the desired quantities. Table 14 presents the average value of heat flux and radial distance, between the array and the plume centerline, from all pairs (T_i,T_{i+1}) and (z_i,z_{i+1}) for several vents. Figure 15 shows the results of the pairwise calculations plotted against height and compared to the results of the calculations of heat flux that assume a radial distance.

Appendix II

To calculate the conductive heat flow anomaly, or missing heat, for the Juan de Fuca Ridge, I averaged the conductive heat flow data reported by Moran and Lister [1987] in 10 km bins along a transect perpendicular to the ridge. Using the half-space cooling model [Turcotte and Schubert, 1982] to calculate the theoretical conductive heat flow for each bin, I determined the heat flow anomaly, q_i, for the i^{th} bin by subtracting the observed conductive heat flow from the predicted conductive heat flow. The total heat flux anomaly Q, or missing heat, is the integral of the heat flow anomaly for each bin from the ridge (x = 0 km) to the perpendicular distance where the heat flow anomaly decays to zero (x = 230 km, see Figure 16) [Sleep and Wolery, 1978]:

$$Q = \int_{x = 0\ km}^{x = 230\ km} (q_{theoretical} - q_{observed})dx \quad . \qquad (30)$$

Using the trapezoid rule for the integration of a discrete function, the total heat flux anomaly is given by

$$Q = D_t\Delta x - 0.5D_0\Delta x, \qquad (31)$$

where D_t is the sum of the heat flow anomalies q_i from 0 km to 230 km (where q_i decays to zero), D_0 is the heat flow anomaly at the ridge crest (x = 1 km is used in the calculations to avoid an infinite heat flow), and Δx is the bin size (10 km). For the Juan de Fuca

Ridge, I calculated the following values: $D_t = 5.0246$ W/m^2, $D_0 = 2.196$ W/m^2, and $Q = 0.039$ MW/m.

Appendix III

The following programs were used to calculate heat flux for the sampled hydrothermal vents. All codes in this appendix are in MATLAB script.

Using the calculation method presented based on temperature and velocity data and an assumed distance between the array and plume centerline (equations 9, 13 and 18), I wrote ventmat.m and its subprograms getnum.m, fiter.m, vfiter.m and inplume.m so I could process each vent sample with ease. The files vvent, flvent, and amb referred to in the programs contain the ALVIN data logger records, the flowmeter records, and deduced ambient temperatures respectively for a single vent sample. The subprograms fiter.m and vfiter.m iteratively calculate the buoyancy flux and virtual height for a given estimated centerline temperature or velocity, exit temperature and height. The subprograms getnum.m and inplume.m calculate the sets of centerline temperature and velocity estimates.

Using the equations presented in appendix I, I wrote the program vsol.m to facilitate the solution for buoyancy flux, the distance between the plume centerline and the array, and the mean centerline temperature.

```
% ventmat.m
%
% script to create matices of temperature anomalies, bouyancy
% flux estimates, and virtual height estimates
%
% load the following input files and set to the given names
% temperature data: eg. vvent = v13b.dat
% velocity data: eg. flvent = fl13b.dat
% ambient means: eg. amb = amb13.dat
%
% parameters
Tmax_Tc_1 = 2.0;     % considered best parameter value
Tmax_Tc_2 = 3.0;
Wc_Wav_1 = 0.43;     % considered best parameter value
Wc_Wav_2 = 0.98;
Tc_Tav_1 = 1.4;
Tc_Tav_2 = 2.0;      % considered best parameter value
Wmax_Wc = 1.65;      % considered best parameter value
z=[11.2 21.3 30.1 39.7 49.5];
T0 = 350;
%
getnum
%
ts(1,:)=TEMP(:,2)';
ts(2,:)=ts(1,:)./Tmax_Tc_1;
ts(3,:)=ts(1,:)./Tmax_Tc_2;
ts(4,:)=CTEMP(:,1)';
ts(5,:)=ts(4,:).*Tc_Tav_1;
ts(6,:)=ts(4,:).*Tc_Tav_2;
ts(7,:)=TEMP(:,1)';
ts(8,:)=ts(7,:).*Tc_Tav_1;
ts(9,:)=ts(7,:).*Tc_Tav_2;
%
vs=[VEL(:,2); VEL(:,2)./Wmax_Wc; CVEL(:,1); ...
    CVEL(:,1).*Wc_Wav_1; CVEL(:,1).*Wc_Wav_2; VEL(:,1); ...
    VEL(:,1).*Wc_Wav_1; VEL(:,1).*Wc_Wav_2];
vs=vs./100;
%
for i=1:9,
        for j=1:5,
                [B0(i,j),z0(i,j)]=fiter(T0,ts(i,j),z(j),'n');
        end
end
%
for i=1:8,
        [vB0(i),vz0(i)]=vfiter(T0,vs(i),z(2)+1,'n');
end
%
```

```
% getnum.m
%
% script to characterize a vent based on temperature and
% velocity data with the coldwater sections removed
for i=1:size(vvent),
        for j=1:5,
                t(i,j) = vvent(i,j+6) - amb(j);
        end
end
t1=inplume(t(:,1),.05,'min');
t2=inplume(t(:,2),.05,'min');
t3=inplume(t(:,3),.05,'min');
t4=inplume(t(:,4),.05,'min');
t5=inplume(t(:,5),.05,'min');
%
TEMP = [mean(t1) max(t1);mean(t2) max(t2);
        mean(t3) max(t3);
        mean(t4) max(t4);mean(t5) max(t5)];
%
v=inplume(flvent(:,2),2,'dis');
VEL = [mean(v) max(v)];
%
% script to characterize a vent based on temperature and
% velocity  data without removing the coldwater sections
for i=1:size(vvent),
        for j=1:5,
                t(i,j) = vvent(i,j+6) - amb(j);
        end
end
t1=t(:,1);
t2=t(:,2);
t3=t(:,3);
t4=t(:,4);
t5=t(:,5);
%
CTEMP = [mean(t1) max(t1);mean(t2) max(t2);
        mean(t3) max(t3);
        mean(t4) max(t4);mean(t5) max(t5)];
%
v=flvent(:,2);
CVEL = [mean(v) max(v)];
%
% EOF
```

```
% implume.m
%
function [output]=inplume(input,margin,key)
% removes from input array values assumed to be outside the
% plume
output=input;
% key tells if data is to be compared to an absolute minimun or
% if data is to be compared to a distance from a zero baseline
if (strcmp(key,'dis'))
        input=abs(input);
end
n=size(input);
low = 0;
out = 0;
k=1;
        for j=1:n,
                last = low;
                if (input(j) <= margin)
                        low = 1;
                        if(last == 1 & out == 0)
                                out = 1;
                                begin(k) = j-1;
                        end
                else
                        low = 0;
                        if(out == 1)
                                out=0;
                                myend(k) = j-1;
                                k=k+1;
                        end
                end
        end
        low = 0;
        if (out == 1)
                out = 0;
                myend(k) = j-1;
                k=k+1;
        end
%
for j=1:(k-1),
        output(begin(k-j):myend(k-j))=[];
end
```

```
% vfiter.m
%
function [B0,z0]=vfiter(T0,V,z,q)
% this function [B0,z0]=fiter(T0,V,z,q) finds the best
% combination of bouyancy flux, B0, and virtual source
% distance, z0, for a given velocity, V,
% exit temperature, T0, and height, z.
b1 = 3.85;          % experimental constant
b4 = 14.29;         % experimental constant
alpha = 1.48e-4;    % coefficient of thermal expansion
g = 10;             % acceleration of gravity
%
MAXITERATIONS = 1000;
iz0 = 0;            % intial value
%
z0=iz0;
for i=1:MAXITERATIONS,
        iz0=z0;
        B0=((V/b1)^3)*(z+z0);
        z0=(b4*B0^(2/3)/alpha/g/T0)^(3/5);
        if (q=='y')
                fprintf('B0 = %10.4e ; z0 = %6.4f \n',B0,z0)
        end
        if ( abs(z0-iz0) < 1e-5 )
                break
        end
end
%
% EOF
```

```
% fiter.m
%
function [B0,z0]=fiter(T0,T,z,q)
% this function [B0,z0]=fiter(T0,T,z) finds the best
% combination of bouyancy flux, B0, and virtual source
% distance, z0, for a given temperature anomaly, T,
% exit temperature, T0, and height, z.
b4 = 14.29;        % experimental constant
alpha = 1.48e-4;   % coefficient of thermal expansion
g = 10;            % acceleration of gravity
%
MAXITERATIONS = 1000;
iz0 = 0;           % intial value
%
z0=iz0;
for i=1:MAXITERATIONS,
        iz0=z0;
        B0=(T*alpha*g*(z+z0)^(5/3)/b4)^(3/2);
        z0=(b4*B0^(2/3)/alpha/g/T0)^(3/5);
        if (q=='y')
                fprintf('B0 = %10.4e ; z0 = %6.4f \n',B0,z0)
        end
        if ( abs(z0-iz0) < 1e-5 )
                break
        end
end
%
% EOF
```

```
% vsol.m
%
function y=vsol(T1,z1,T2,z2)
% function y=vsol(T1,z1,T2,z2)
% solves for radial distance from centerline given temp.
% at two vertiacally spaced thermistors
a=.112;
c1 = 9.7e3;
c2=2.94e9;
M=1e6;
%
Tr=T1/T2;
zr=z1/z2;
%
% FIRST SOLUTION:
r=((a^2)*log(Tr*(zr^(5/3)))/(1/(z2^2)-1/(z1^2)))^.5;
%
Tc1=T1.*exp((1/(a^2)).*((r/z1).^2));
Tc2=T2.*exp((1/(a^2)).*((r/z2).^2));
%
H1=((Tc1/c1)^(3/2))*(z1^(5/2));
H1=c2*H1/M;
%
% SECOND SOLUTION
g=zr^(-2); v=g/(g-1); n=1/(g-1);
%
%
Bo=(((T2^v)/(T1^n))^(3/2))*(c1^(-3/2))*(((z2^v)/(z1^n))^(5/2));
%
H2=Bo*c2/M;
%
Tc3=c1*(Bo^(2/3))/(z1^(5/3));
Tc4=c1*(Bo^(2/3))/(z2^(5/3));
%
r2=z2*a*((log(Tc4/T2))^.5);
%
fprintf('radius:  %5.2f m \n',r)
fprintf('heat flux 1: %5.1f MW \n',H1)
fprintf('  %5.2f C  at %5.1f m\n',Tc1,z1)
fprintf('  %5.2f C  at %5.1f m\n',Tc2,z2)
fprintf('heat flux 2: %5.1f MW \n',H2)
fprintf('  %5.2f C  at %5.1f m\n',Tc3,z1)
fprintf('  %5.2f C  at %5.1f m\n',Tc4,z2)
fprintf('radius from 2:  %5.2f m \n',r2)
% EOF
```

Appendix IV

Before attempting to characterize the temperature and velocity data from each dive, I extracted it from digital records. The ALVIN data logger recorded navigation data and time in the appropriate units, but my array data (5 thermistors, 1 transmissometer, 1 platinum thermistor) was recorded in frequencies. For the thermistors, the frequency was converted to resistance and then to temperature using laboratory calibrations. The coefficients and equations used are presented in Table 15. The flowmeter recorded its data on an analog tape that was then converted to digital data. I used the program rtpmain.c and its subprograms, written in the C language, to convert the recorded data counts to the appropriate units.

```
/* program rtpmain.c    */

/* main program to run rtp software */
/* rtp subroutines provided by Melora Park */
/* remainder by Karen G. Bemis */

#include <stdio.h>
#include <ctype.h>
#include <math.h>

#define ZERO 0
#define SAMP 14.0625

/*************************************************************/
/* subroutine openinfile opens file for reading              */
FILE *openinfile(name1)
char *name1;
{
FILE *infile;
int i,leng=110;
char dummy[80];

infile = fopen(name1,"r");
if (infile == NULL)
        printf("infile = Null");

for(i=0;i<11;i++) {    /* to read through first 10 lines (header info) */
       fgets(dummy,leng,infile);
/*      printf("dummy : %s \n",dummy);*/
}

return(infile);
}

/*************************************************************/
/* subroutine openoutfile opens file for writing             */
FILE *openoutfile(name2)
char *name2;
{
FILE *outfile;

outfile = fopen(name2, "w");
if (outfile == NULL)
        printf("outfile = null");

return(outfile);
}

/*******************************************************/
/* subroutine reads record into string                 */
readrecord(string, infile)
char string[];
FILE *infile;
{
int key=0,leng=55,c;

if( (c = fgets(string,leng,infile)) != ZERO) {
/*      printf("c= %d\n",c);*/
        key = 1;
}
/*printf("string, key %s, %d",string,key);*/

return(key);
}
```

```
/*******************************************************/
/* subroutine outputs decoded record, as variables,  */
/* to a file in ascii format                          */
writerecord(out,sec,u,w1,v,w2,cond,comp,pres,temp,tilte,tiltn)
FILE *out;
float sec;
float u,w1,v,w2,cond,comp,pres,temp,tilte,tiltn;
{

fprintf(out,
"%7.1f %10.3f %10.3f %10.3f %10.3f %10.3f %4.0f %10.3f %10.3f %5.0f %5.0f\n",
sec,u,w1,v,w2,cond,comp,pres,temp,tilte,tiltn);
return;
}

/*******************************************************/
/* subroutine closes files                             */
closefile(in,out)
FILE *in,*out;
{
close(in);
close(out);
return;
}

/*******************************************************/
/* MAIN PROGRAM:                                       */
/* p1 and p2 are runtime parameters to be files names  */
/*******************************************************/
main(argc,argv)
int argc;
char *argv[];
{
FILE *in, *out;
FILE *openinfile(),*openoutfile();
char *p1, *p2, *p3;
int i=0,key=0,reset;
float sec;

char string[55];
int rec;
float u,w1,v,w2,cond,comp,pres,temp,tilte,tiltn;

p1 = argv[1];
p2 = argv[2];
printf("filenames are %s %s \n", p1, p2);
p3 = argv[3];
printf("reset time in seconds is %s \n",p3);
reset = atoi(p3);

out = openoutfile(p2);
in = openinfile(p1);

while( (key = readrecord(string,in)) != ZERO) {
/*      printf("key = %d \n",key);*/
        i=i+1;
        rtp1cal(string,&rec,&u,&w1,&v,&w2,&cond,&comp,&pres,&temp,&tilte,&tiltn,p2);
        sec = rec*SAMP + reset;
        writerecord(out,sec,u,w1,v,w2,cond,comp,pres,temp,tilte,tiltn);
        if(i>9999)
                break;
}

closefile(in,out);

}
```

```
/* rtp1cal.h  */

/*  Include file that contains calibrations constants for
       Real_time profiler --- rtp1

       June 23, 1989
*/

#define RS      4498.55          /* standard resistance */
#define TS      14.0625          /* sample interval */
#define K       2.0              /* # multiplexed sensors in circuit */
#define AZ      273.15           /* kelvin to celcius */
#define CM_PER_CNT      7.5      /* cm per counts for rotor conversion*/
#define PI      3.1415926
#define THREESIXTY      360.

#define R1_W    9038.6           /* temperature conversion */
#define R2_W    3998.8
#define F1_W    188.11
#define F2_W    977.54
#define TA_W    0.108620e-02
#define TB_W    0.26385506e-03
#define TC_W    0.139657e-06

#define FCONDT  3.515625         /* conductivity sample interval cell #131 */
#define CA      5.37479441e-08   /* conductivity cal constants */
#define CB      5.557379e-01
#define CC      -8.5051738e-03
#define CD      2.53405111e-04
#define M       6.7

#define THETA   -144.            /* compass cal constants */
#define THETC   -6.
#define THETD   -23.
#define THETAE  7.

#define FPT     5.2734375;       /* pressure sample interval */
#define PA      0.225            /* pressure cal constants */
#define PB      2.57927

#define TGAIN   10.              /* tilt gain factor */

#define NEG24           0x0800000       /* 24bit fall over from positive to nega
tive */
#define EXTEND24        0xFF000000      /* 24 to 32 bit sign extend */
#define NEG16           0x08000         /* 16bit fall over from positive to nega
tive */
#define EXTEND16        0xFFFF0000      /* 16 to 32 bit sign extend */
#define NEG8            0x080           /* 8 bit fall over from positive to nega
tive */
#define EXTEND8         0xFFFFFF00      /* 8 to 32 bit sign extend */

#define REC1 1517
#define REC2 1569
#define SHIFT 45
```

```
/*  subroutine rtp1cal.c

        converts o real-time profiler — rtp1
        to engineering units.  The string that is passed
        to this routine must be of the following specific format:
                                #characters
                record number    4
                rotor 1 (r1)     4
                rotor 2 (w1)     4
                rotor 3 (r2)     4
               rotor 4 (w2)     4
                conductivity     4
                compass          2
                pressure         6
               tilt east        6
                temperature      6
               tilt north       6

                total            50

        June 23, 1989   M.Park
*/

#include <stdio.h>
#include <errno.h>
#include <math.h>
#include "rtp1cal.h"

#define ZERO 0

int rtp1cal(string,rec,u,w1,v,w2,cond,comp,pres,temp,tilte,tiltn,dive)

char string[55];
int *rec;
float *u,*w1,*v,*w2;
float *cond,*comp,*pres,*temp;
float *tilte,*tiltn;
char *dive;

{
        int rec_num1,rec_num0;
        int cr1,cw1,cr2,cw2;
        int cpres,ctemp;
        int ccond,ccomp;
        int ctlte,ctltn;
        int uv_rtp();
        float w_rtp();
        float cd_rtp();
        float cp_rtp();
        float p_rtp();
        float t_rtp();
        float tilt();
        int rec_err = 0;
        int start = 0;
  int ret;
        static int lastccond = 0;
        static float lasttemp = 0;
        static float lastpres = 0;
        static int lastrec = 0;
        float rate_of_pressure_change();
        int hold;
        /*register int j;*/

/*      printf("string is %s \n",string);*/

        if ( string[1] == 'P') {
                *rec=0;
                *u=0.;
                *w1=0.;
         *v=0.;
```

```
                *w2=0.;
                *cond=0.;
                *comp=0.;
                *pres=0.;
                *temp=0.;
                *tilte=0.;
                *tiltn=0.;
                return(-1);

        }

        else {
                ret = sscanf(string,"%4x%4x%4x%4x%4x%4x%2x%6x%6x%6x%6x",
        rec,&cr1,&cw1,&cr2,&cw2,&ccond,&ccomp,&cpres,&ctlte,&ctemp,&ctltn);
        }

        if (ret != 11 ) {
                *rec=0;
         *u=0.;
                *w1=0.;
                *v=0.;
                *w2=0.;
                *cond=0.;
                *comp=0.;
                *pres=0.;
                *temp=0.;
                *tilte=0.;
                *tiltn=0.;
                return(-1);
        }

/*  get calibrated values */
        *temp = t_rtp(ctemp);
        *comp = cp_rtp(ccomp);

        if( strcmp(dive,"fl2113.out") == ZERO) {  /* added by kgb */
                hold = ccond;
                ccond = ccond - lastccond;
                lastccond = hold;
                uv_rtp(cr1,cr2,*comp,u,v);
                *w1 = w_rtp(cw1);
                *w2 = w_rtp(cw2);
        }
        else if ( strcmp(dive, "fl2112.out") == ZERO) {  /* added by kgb */
                hold = ccond;
                ccond = ccond - lastccond;
                lastccond = hold;
                *w2 = w_rtp(cw2);
        }
        else {
                uv_rtp(cr1,cr2,*comp,u,v);
                *w1 = w_rtp(cw1);
                *w2 = w_rtp(cw2);
        }

        *cond = cd_rtp(ccond,*temp);
        lasttemp = *temp;

     *pres = p_rtp(cpres);
        *tilte = tilt(ctlte);
        *tiltn = tilt(ctltn);

/*      if( strcmp(dive,"fl2113.out") == ZERO) {*/
                if((*rec >= REC1) && (*rec <= REC2))
                        datacheck(ccond,*cond,*comp,cr1,cr2,*u,*v);
/*      }*/

        if(*rec > 1 ) {
           *w1 = *w1 -  rate_of_pressure_change(*rec,lastrec,*pres,lastpres);
        }
```

```
        lastpres = *pres;
        lastrec = *rec;

        return(0);

}
/*  subroutines rtpalgo.c

        Calibration algorithms to convert rtp0 or rtp1 to scientific units
        For use with routines rtp1cal.c and rtp0cal.c

        float w_rtp(counts)             returns w rotor velocity cm/sec
        float t_rtp(counts)             returns temperature deg C
        float p_rtp(counts)             returns pressure in decibars
        float cd_rtp(counts,temp)       returns conductivity in mmhos/cm
                                        temperature from above is input
        float cp_rtp(counts)            returns compass in degress
        float tilt(counts)              returns tilts in degrees
        int uv_rtp(r1,r2,deg,evec,nvec)
                                        returns by address the north and east
                                        vectors, given counts for u and v and compass

        June 23, 1989   M.Park

*/

/*****************************************************************************
        w rotor counts (cm/sec):
*/
float w_rtp(counts)
int counts;
{
        float x;

        if ( counts > NEG16 )
                counts = counts|EXTEND16;

        x = counts * CM_PER_CNT/TS;
        return(x);
}
/*****************************************************************************
        water temperature (deg C):
        Returns computed value or 0 if errflag negative.
        if errflg = -1          argument 0 or negative to log function
        if errflg = -2          expression over or under flows
*/
float t_rtp(counts)
int counts;
{
        double x,y;                     /* working variables */
        double ratio1,ratio2;
        double bk,pk,qk;
        double tim;
        double f,r,t;
        int errflg = 0;
        double sd;                      /* switch delay */
        double val;

        if ( counts > NEG24 )
                counts = counts | EXTEND24;

        sd = 450./256.;
        ratio1 = R1_W/RS;
        ratio2 = R2_W/RS;
        bk = 1./(ratio2 + 1.);
        x = 1./(ratio1 + 1.);
        pk = (F2_W - F1_W) / (bk - x);
        y = F1_W/pk;
        qk = x - y;
        tim = TS/K - sd;
```

```
        f = counts/tim;
        x = 1./(f/pk + qk);
        r = RS * (x - 1.0);
        if ( r <= 0.)
                return(9999.);

        x =  log(r);
    /*if ( errno == EDOM) {
                errflg = -1;
                return(9999.);
        }*/
        y = x*x*x;
     /*if ( errno == ERANGE) {
                errflg = -2;
                return(9999.);
        }*/
        t = 1./(TA_W + TB_W*x + TC_W*y);
        return((float)(t-AZ));
}
/*****************************************************************************
        pressure decibars:
*/
float p_rtp(counts)
int counts;

{
        float x;
        float f;

        if ( counts > NEG24 )
                counts = counts | EXTEND24;

        f = counts/FPT;
        x = PA + PB*f;
        return(x);
}
/*****************************************************************************
        conductivity (mmhos/cm):
*/
float cd_rtp(counts,temp)
int counts;
float temp;
{
        float x;
        float f;
        double fex;

        f = (counts/FCONDT)*1.0e-03;
        if( f < 0 )
                return(9999.);
        fex = pow((double)f,(double)M);

        x = CA*fex + CB*f*f + CC + CD*temp;
        return(x);
}
/*****************************************************************************
        compass (degrees):
*/
float cp_rtp(counts)
int counts;
{
        float x;
        float thetab;
        double rad,rad2;

        thetab = counts * THREESIXTY/255.;
        rad = (thetab + THETD) *2* PI/THREESIXTY;
        rad2 = 2*(thetab) * PI/THREESIXTY;
        x = THETA + thetab + THETC*cos(rad) + THETAE*sin(rad2);
        return(x);
}
```

```
/*****************************************************************************
        east and north vectors (cm/sec)
        do instantaneous compass calculation for now
*/
int uv_rtp(r1,r2,deg,evec,nvec)
int r1,r2;
float deg;
float *evec,*nvec;
{
        float x;
        double rad;

        if ( r1 > NEG16 )
                r1 = r1 | EXTEND16;
        if ( r2 > NEG16 )
                r2 = r2 | EXTEND16;

        rad = 2 * deg * PI/THREESIXTY;
        *nvec = (r2*cos(rad) + -r1*sin(rad))*CM_PER_CNT/TS;
        *evec = (r1*cos(rad) + r2*sin(rad))*CM_PER_CNT/TS;
        return;
}

/*****************************************************************************
        tilt sensors (degrees):
*/
float tilt(counts)
int counts;
{
       float x;

        if ( counts > NEG24 )
                counts = counts | EXTEND24;
        x = counts/TGAIN;
        return(x);

}

/*************************************************************/
/* subroutine outputs section of data for hand check of the */
/* decoding algorithm            (added by kgb)              */
datacheck(ccond,cond,comp,cr1,cr2,u,v)
int ccond,cr1,cr2;
float cond,comp,u,v;
{
printf("%d %f %f %d %d %f %f\n",ccond,cond,comp,cr1,cr2,u,v);
return;
}
```

```
/* subroutine rate.c    */

/*********************************************************/
/* subroutine calculates the rate of pressure change     */

#include <stdio.h>
#include <math.h>

#define PTOZ 10/9.81/1.039    /* pressure to depth conversion factor */
#define RI 14.0625   /* sampling interval */

float rate_of_pressure_change(rec,last_rec,pres,last_pres)
int rec, last_rec;
float pres, last_pres;
{
float dq,dz,dp,rate,dzdt;

dq = rec - last_rec;
printf("dq %f\n",dq);
dp = (pres - last_pres)/dq;
/*printf("dp %f \n",dp);*/
dz = dp*PTOZ;
rate = dz/RI;
dzdt = rate*100;
/*printf("dzdt %f\n",dzdt);*/

return(dzdt);
}
```

Table 1. Heat Anomaly

Ridge	Half-Spreading Rate (mm/yr)	Heat Anomaly (MW/m)
Galapagos	30	0.009
EPR	61	0.127
MAR	20	0.056
JdF	30	0.039

Except for the Juan de Fuca Ridge, heat flux data is quoted from Sleep and Wolery, 1978.

Table 2. Previous Estimates of the Heat Flux From Hydrothermal Vents

Source	Location†	Heat Flux (MW)	Estimation Basis
Macdonald, et. al.,1980	EPR-21°N	60 ± 20	exit conditions
Little, et. al, 1988	EPR-11°N	2.76	array-simple plume
		3.40	array-nonlinear plume
Baker and Massoth, 1987	JdF-SS	580 ± 351	advective flux -u.w.c.††
	JdF-ES	1700 ± 1100	advective flux - u.w.c.
Crane, et. al., 1985	JdF-SS	3024 - 302,400	advective flux - u.w.c.
		2096	line source
	JdF-ES	1260 - 126,000	advective flux - u.w.c.
		1133	line source
Rosenburg, et. al., 1988	JdF-ES	1000-5000	radon/heat ratio

† EPR = East Pacific Rise; JdF = Juan de Fuca Ridge; ES = Endeavor Segment; SS = Southern Segment.

†† u.w.c. = upper water column.

Table 3. Estimates of the Parameters in Theoetical Descriptions of Plumes

Constant	Fitted Values		
	Papanicolaou and List	Previous	Equation
b_w/z	0.105	0.100	$w=w_c\exp(-(r/b_w)^2)$
b_c/z	0.112	- -	$C=C_c\exp(-(r/b_w)^2)$
b_1	3.85	4.7	$w_c=b_1(B_0/z)^{1/3}$
b_2	0.290	0.35	$M_0=b_2(B_0^2z_0^4)^{1/3}$
b_3	0.140	0.15	$\mu=b_3(B_0z^5)^{1/3}$
b_4	14.29	9.1	$T_c=b_4(B_0^2/z^5)^{1/3}/a/g$

Table 4. Empirical Ratios of maximum and mean parameters.

Relation†	Observed Ratios	Reference
Tmax/Tc	1.5-2.5	Papanicolaou and List, 1987
Cmax/Cc	2.0-3.0	Papanicolaou and List, 1988
	4.0	Papantoniou and List, 1989
Wmax/Wc	1.65	Papanicolaou and List, 1988

† T=temperature; C=concentration; and W=vertical velocity.

Table 5a. Mean and Maximum Values from Array Data: Endeavor Segment

Dive-Vent	Start (h:m)	Stop (h:m)	z(T)† (m)	T_{max} (°C)	T_{cold} (°C)	T_{hot} (°C)	V_{max} (m/s)	V_{cold} (m/s)	V_{hot} (m/s)	X†† (m)	Y†† (m)
2112-E	12:57	13:11	40	0.32	0.13	0.17	0.176	0.097	0.097	4934	6163
2112-F	13:18	13:23	40	0.21	0.06	0.07	0.112	0.031	0.052	4937	6166
2112-K	15:07	15:29	40	0.97	0.27	0.30	0.395	0.119	0.140	4924	6154
2113-B	10:33	11:17	40	1.58	0.61	0.63	0.416	0.124	0.127	4984	6157
2113-E	11:42	11:54	50	1.28	0.39	0.40	0.235	0.134	0.134	4965	6147
2113-Q	12:03	12:11	40	1.29	0.28	0.28	0.133	0.077	0.077	4974	6156
2113-R	12:15	12:26	40	1.35	0.51	0.61	0.304	0.125	0.125	4984	6159
2113-S	13:39	13:45	30	0.84	0.42	0.44	0.197	0.132	0.132	5042	6238
2113-T	13:55	14:12	50	0.16	0.00	0.08	0.059	0.000	0.030	5045	6247
2114-A	10:25	11:00	40	0.40	0.10	0.10	0.240	0.018	0.017	4937	6017
2114-B	11:49	12:38	50	0.32	0.06	0.11	0.181	0.064	0.067	4884	5998
2114-C1	12:41	12:52	50	0.12	0.04	0.06	0.101	0.016	0.023	4879	5994
2114-C2	12:52	12:58	40	0.14	0.01	0.07	0.240	0.076	0.076	4889	5994
2114-C3	12:59	13:03	50	0.12	0.05	0.07	0.053	-.007	-.017	4894	6005
2114-C4	13:04	13:07	20	0.28	0.05	0.11	0.043	0.020	0.032	4890	6002
2114-D	13:51	14:08	50	0.19	0.02	0.10	0.058	0.020	0.028	4886	6001
2114-F	15:06	15:28	20	3.11	0.62	0.71	0.272	0.069	0.080	4920	6146
2114-Q	10:07	10:24	50	0.08	0.05	0.06	0.197	-.029	-.029	4930	6024
2114-S	11:05	11:14	40	0.25	0.12	0.12	0.080	0.021	0.021	4928	6016
2114-T	11:17	11:20	20	2.58	0.85	0.85	0.187	0.048	0.048	4938	6010
2114-V	13:14	13:21	20	0.39	0.05	0.12	0.075	0.019	0.038	4897	5985
2115-A	12:25	12:40	50	0.29	0.10	0.12	0.064	0.015	0.022	4987	6212
2115-B	12:57	13:37	20	0.52	0.13	0.21	0.141	0.014	0.018	5046	6242
2115-C	13:39	14:04	20	1.67	0.23	0.47	0.341	0.053	0.105	5047	6246
2115-D	14:19	14:36	40	0.57	0.11	0.19	0.315	0.110	0.110	5038	6248
2115-F	14:42	14:49	30	0.65	0.19	0.19	0.210	0.092	0.092	5035	6247
2115-H	15:06	15:20	50	0.91	0.17	0.29	0.187	0.050	0.066	4988	6180
2115-J	15:24	15:36	20	3.04	0.97	1.36	0.432	0.159	0.171	4994	6182
2115-Q	11:46	11:54	50	0.15	0.08	0.09	0.176	0.031	0.035	5044	6251
2116-D	10:55	11:11	50	0.13	0.06	0.07	0.059	0.016	0.026	7046	7360
2116-G	13:05	13:09	50	0.60	0.23	0.25	0.395	0.105	0.128	6973	7304

†height of thermistor for which temperatures are quoted.
††x-y locations in the transponder net - Figure 1 shows the location of the area in latitude and longitude while Figure ? uses transponder net coordinates.
Temperatures are anomalies with respect to ambient temperature; velocites are absolute values.

Table 5b. Mean and Maximum Values from Array Data: Southern Segment

Dive-Vent	Start (h:m)	Stop (h:m)	z(T)† (m)	T_{max} (°C)	T_{cold} (°C)	T_{hot} (°C)	V_{max} (m/s)	V_{cold} (m/s)	V_{hot} (m/s)	X†† (m)	Y†† (m)
2117-A	10:05	10:14	50	0.17	0.01	0.07	-	-	-	11822	12867
2117-B	10:43	10:48	50	0.18	-	0.09	-	-	-	11874	13138
2117-C	11:34	11:48	50	0.21	0.04	0.08	-	-	-	11883	13195
2117-D	11:54	11:59	50	0.09	0.05	0.05	-	-	-	11940	13230
2117-E	12:02	12:08	50	0.09	0.05	0.06	-	-	-	11948	13219
2117-F	12:10	12:15	50	0.07	0.04	0.05	-	-	-	11933	13207
2117-G	12:21	12:27	50	0.08	0.04	0.06	-	-	-	11933	13210
2117-H	12:35	13:01	40	0.24	0.05	0.06	-	-	-	11925	13225
2117-I	13:07	13:13	50	0.06	0.03	0.05	-	-	-	11920	13225
2117-J	13:17	13:22	50	0.19	0.02	0.08	-	-	-	11910	13214
2117-K	15:27	15:42	40	0.37	0.00	0.09	-	-	-	12145	14136
2118-D	13:31	13:39	30	0.12	0.04	0.08	0.037	0.025	0.026	11300	11300
2118-E	13:46	13:48	10	0.34	0.18	0.25	0.016	-.002	-.029	11300	11300
2118-F	14:10	14:31	30	0.08	0.02	0.06	0.021	-.003	-.015	11316	11366
2118-G	14:45	14:50	20	0.06	0.00	0.05	0.000	-.022	-.030	11317	11377
2118-H	15:01	15:12	30	0.09	0.04	0.06	0.016	-.015	-.029	11309	11383
2119-A	10:15	10:25	20	0.28	0.10	0.14	0.059	0.004	0.006	12878	15989
2119-B	10:32	10:41	30	0.13	0.04	0.08	0.071	0.004	0.010	12878	15989
2119-C	13:40	13:45	10	0.37	0.27	0.27	0.050	0.007	0.009	12770	15617
2119-D	13:51	14:00	30	0.07	0.03	0.06	0.058	0.002	0.004	12765	15613
2119-E	14:28	14:34	10	0.80	0.16	0.33	0.034	-.004	-.005	12710	15585
2119-F	14:36	14:44	40	0.09	0.02	0.06	0.034	-.001	-.002	12706	15585
2120-A	11:10	11:17	20	0.19	0.03	0.08	0.034	-.001	-.009	11313	11333
2120-B	11:50	12:03	40	0.34	0.16	0.16	0.116	0.014	0.017	11294	11328
2120-C	12:31	12:37	40	0.16	0.08	0.10	0.135	0.027	0.032	11321	11396
2120-D	13:50	14:12	30	0.29	0.02	0.17	0.093	-.013	-.016	11309	11391
2120-E	14:32	14:38	20	0.11	0.01	0.07	0.157	0.031	0.033	11305	11374
2120-F	14:45	14:56	30	0.32	0.06	0.17	0.034	-.019	-.023	11309	11380
2120-G	15:38	15:43	10	0.78	0.25	0.25	0.197	0.121	0.121	11311	11466
2121-A	09:22	09:29	40	0.55	0.16	0.19	0.128	0.055	0.059	11895	13206
2121-B	09:33	09:43	40	1.21	0.33	0.33	0.080	0.036	0.042	11881	13207
2121-C	09:47	09:56	50	0.28	0.07	0.09	0.080	0.028	0.034	11863	13192
2121-D	10:23	10:36	10	4.29	0.39	1.07	0.085	0.003	0.021	11943	13234
2121-E	11:32	11:40	20	1.11	0.45	0.54	0.107	0.046	0.061	11945	13250
2121-F	12:39	12:51	10	4.31	0.96	0.97	0.005	-.004	-.019	12159	14118

†height of thermistor for which temperatures are quoted.
††x-y locations in the transponder net - Figure 1 shows the location of the area in latitude and longitude while Figures 2 and 3 uses transponder net coordinates.

Table 6a. Heat Flux Estimates based on the Array Temperature Data: Endeavor Segment

Dive-Vent	Observed†	Duration (min)	H(raw)†† (MW)	$H(T_{max})$ (MW)	$H(T_{hot})$ (MW)	$H(T_{cold})$ (MW)
2112-E	smoker?	12	1.5	1.5	6.6	4.4
2112-F	smokers	4	0.5	0.8	1.7	1.4
2112-K	smokers	11	4.7	8.1	15.8	13.4
2113-B	smoker	37	16.2	17.1	49.6	47.2
2113-E	smoker	12	8.2	12.4	24.6	23.6
2113-Q	smoker	8	4.9	12.5	14.2	14.2
2113-R	smoker	11	12.3	13.4	47.2	35.7
2113-S	flange	6	4.6	3.3	14.3	13.3
2113-T	smoker	15	0.0	0.9	3.6	0.0
2114-A	smoker	34	1.0	2.1	3.0	3.0
2114-B	smoker	47	0.8	2.6	5.8	2.3
2114-C1	smoker	11	0.4	0.6	2.3	1.3
2114-C2	smoker	6	0.0	0.4	1.7	0.1
2114-C3	shim.wat.	4	0.6	0.6	2.9	1.8
2114-C4	shim.wat.	7	0.1	0.3	0.7	0.2
2114-D	smoker	16	0.2	1.2	5.0	0.4
2114-F	smoker	21	3.4	9.9	12.2	9.9
2114-Q	smoker	17	0.6	0.3	2.3	1.8
2114-S	smoker	9	1.4	1.0	3.9	3.9
2114-T	smoker	3	5.5	7.4	16.2	16.2
2114-V	smoker?	7	0.1	0.4	0.8	0.2
2115-A	worms	14	1.8	2.2	6.6	5.0
2115-B	smoker	39	0.3	0.6	1.9	0.9
2115-C	smoker	24	0.7	3.8	6.4	2.1
2115-D	smoker	16	1.2	3.6	7.9	3.4
2115-F	smoker	7	1.4	2.2	4.0	4.0
2115-H	smoker	14	3.9	12.5	25.4	11.2
2115-J	smoker	12	6.8	9.6	33.9	19.9
2115-Q	smoker	8	1.3	0.8	4.3	3.6
2116-D	shim.wat.	15	0.8	0.7	2.9	2.3
2116-G	smoker	4	6.2	6.6	20.2	17.8

† Lists the observed hydrothermal phenomena - all numbers presume the existance of a smoker.

†† H(raw) = heat flux calculated using T_{cold} rather than first estimating T_c (time-averaged centerline temperature) from T_{cold}.

Table 6b. Heat Flux Estimates based on the Array Temperature Data: Southern Segment

Dive-Vent	Observed†	Duration (min)	H(raw)†† (MW)	$H(T_{max})$ (MW)	$H(T_{cold})$ (MW)	$H(T_{hot})$ (MW)
2117-A	worms	11	0.1	1.0	2.9	0.2
2117-B	shim. water	5	0.0	1.1	4.3	0.0
2117-C	smokers	14	0.4	1.3	3.6	1.3
2117-D	smoker	5	0.6	0.4	1.8	1.8
2117-E	smoker	6	0.6	0.4	2.3	1.8
2117-F	smoker	5	0.4	0.3	1.8	1.3
2117-G	smoker	6	0.4	0.3	2.3	1.3
2117-H	smoker	26	0.4	1.0	1.4	1.0
2117-I	smoker	6	0.3	0.2	1.8	0.8
2117-J	smokers	5	0.2	1.2	3.6	0.4
2117-K	spires	15	0.0	1.9	2.5	0.0
2118-D	smoker	8	0.1	0.2	1.1	0.4
2118-E	spires	2	0.1	0.1	0.5	0.3
2118-F	smoker	21	0.0	0.1	0.7	0.1
2118-G	smoker	5	0.0	0.0	0.2	0.0
2118-H	smoker	11	0.1	0.1	0.7	0.4
2119-A	sediment	10	0.2	0.3	1.0	0.6
2119-B	sediment	9	0.1	0.2	1.1	0.4
2119-C	smoker	5	0.2	0.1	0.6	0.6
2119-D	smoker	9	0.1	0.1	0.7	0.2
2119-E	smoker	6	0.1	0.3	0.8	0.3
2119-F	smoker	8	0.1	0.2	1.4	0.3
2120-A	dust	7	0.0	0.1	0.4	0.1
2120-B	smoker	13	2.1	1.6	6.0	6.0
2120-C	spires	6	0.7	0.5	3.0	2.1
2120-D	smoker	22	0.0	0.7	3.3	0.1
2120-E	smokers	6	0.0	0.1	0.4	0.0
2120-F	smokers	11	0.2	0.8	3.3	0.7
2120-G	smokers	5	0.2	0.3	0.5	0.5
2121-A	smokers	7	2.1	3.4	7.9	6.0
2121-B	smokers	10	6.3	11.4	18.3	18.3
2121-C	smokers	9	1.0	2.1	4.3	2.9
2121-D	smokers	13	0.4	3.5	4.9	1.0
2121-E	smoker	8	2.1	2.0	8.0	6.0
2121-F	smoker	12	1.4	3.5	4.2	4.1

† Lists the observed hydrothermal phenomena - all numbers presume the existance of a smoker.

†† Heat(raw) = heat flux calculated using T_{cold} rather than first estimating T_c (time-averaged centerline temperature) from T_{cold}..

Table 7. Vent 2113-E Black smoker near (4965,6167)

	Observations				Assumed Radii			Calculated Radii†		
i	z_i (m)	T_{max} (°C)	T_{cold} (°C)	T_{hot} (°C)	$H(T_{raw})$ (MW)	$H(T_{max})$ (MW)	$H(T_{hot})$ (MW)	r (m)	T_c (°C)	H (MW)
1	11.5	3.10	0.68	0.86	0.8	2.1	3.5	1.37	2.83	6.7
2	21.4	1.24	0.48	0.50	2.3	2.4	6.6	2.07	1.18	8.7
3	30.7	1.02	0.43	0.43	4.8	4.4	13.8	2.36	0.75	10.6
4	40.4	1.28	0.39	0.40	8.2	12.4	24.6	2.47	0.56	13.5
5	49.9	0.71	0.24	0.27	6.6	8.5	22.8	2.14	0.31	9.6

† average values from the table of calculations based on T_{hot} below.

ratio: T_i/T_{i+1} (°C)	r (m)	H (MW)	Tc_i (°C)	Tc_{i+1} (°C)
T_4/T_5	0.00††	6.8	0.36	0.25
T_3/T_5	2.56	10.4	0.75	0.33
T_2/T_5	2.37	9.9	1.32	0.32
T_1/T_5	1.50	8.5	3.35	0.29
T_3/T_4	3.28	17.8	1.07	0.68
T_2/T_4	2.58	13.2	1.60	0.55
T_1/T_4	1.55	9.6	3.65	0.45
T_2/T_3	2.24	8.6	1.20	0.66
T_1/T_3	1.35	5.7	2.58	0.50
T_1/T_2	1.07	3.1	0.61	1.72

†† actual value is imaginary and resultant calculations are not included in the averages above.

Table 8a. Heat Flux Estimates based on the Array Velocity Data: Endeavor Segment

Dive-Vent	Observed†	Duration (min)	$H(V_{raw})$ (MW)	$H(V_{max})$ (MW)	$H(V_{hot})$ (MW)	$H(V_{cold})$ (MW)
2112-E	smoker?	12	1.0	1.4	13.2	13.2
2112-F	smokers	4	0.0	0.3	2.0	0.4
2112-K	smokers	11	1.9	15.8	40.4	24.5
2113-B	smoker	37	2.1	18.5	30.0	27.8
2113-E	smoker	12	2.7	3.3	35.3	35.3
2113-Q	smoker	8	0.5	0.6	6.5	6.5
2113-R	smoker	11	2.2	7.1	28.5	28.5
2113-S	flange	6	2.6	1.9	33.7	33.7
2113-T	smoker	15	0.0	0.1	0.4	0.0
2114-A	smoker	34	0.0	3.5	0.1	0.1
2114-B	smoker	17	0.3	1.5	4.3	3.7
2114-C1	smoker	11	0.0	0.3	0.2	0.1
2114-C2	smoker	6	0.5	3.5	6.3	6.3
2114-C3	shim.wat.	4	0.0	0.0	0.1	0.0
2114-C4	shim.wat.	7	0.0	0.0	0.5	0.1
2114-D	smoker	16	0.0	0.0	0.3	0.1
2114-F	smoker	21	0.4	5.1	7.3	4.7
2114-Q	smoker	17	0.0	1.9	0.3	0.3
2114-S	smoker	9	0.0	0.1	0.1	0.0
2114-T	smoker	3	0.1	1.6	1.6	1.6
2114-V	smoker?	7	0.0	0.1	0.8	0.1
2115-A	worms	14	0.0	0.1	0.1	0.0
2115-B	smoker	39	0.0	0.7	0.1	0.0
2115-C	smoker	24	0.2	10.1	16.7	2.1
2115-D	smoker	16	1.5	7.9	19.3	19.3
2115-F	smoker	7	0.9	2.3	11.2	11.2
2115-H	smoker	14	0.1	1.6	3.9	1.8
2115-J	smoker	12	4.5	20.7	74.8	59.8
2115-Q	smoker	8	0.0	1.4	0.6	0.4
2116-D	shim.wat.	15	0.0	0.1	0.2	0.1
2116-G	smoker	4	1.3	15.8	30.7	16.7

†lists the observed hydrothermal phenomena - all numbers presume the existance of a smoker.

Table 8b. Heat Flux Estimates based on the Array Velocity Data: Southern Segment

Dive-Vent	Observed†	Duration (min)	$H(V_{raw})$ (MW)	$H(V_{max})$ (MW)	$H(V_{hot})$ (MW)	$H(V_{cold})$ (MW)
2118-D	smoker	8	0.02	0.01	0.25	0.22
2118-E	spires	2	0.00	0.00	0.00	0.00
2118-F	smoker	21	0.00	0.00	0.00	0.00
2118-G	smoker	5	0.00	0.00	0.00	0.00
2118-H	smoker	11	0.00	0.00	0.00	0.00
2119-A	sediment	10	0.00	0.05	0.00	0.00
2119-B	sediment	9	0.00	0.09	0.01	0.00
2119-C	smoker	5	0.00	0.03	0.01	0.00
2119-D	smoker	9	0.00	0.05	0.00	0.00
2119-E	smoker	6	0.00	0.01	0.00	0.00
2119-F	smoker	8	0.00	0.01	0.00	0.00
2120-A	dust	7	0.00	0.01	0.00	0.00
2120-B	smoker	13	0.00	0.39	0.07	0.04
2120-C	spires	6	0.02	0.61	0.46	0.28
2120-D	smoker	22	0.00	0.20	0.00	0.00
2120-E	smokers	6	0.03	0.96	0.50	0.42
2120-F	smokers	11	0.00	0.01	0.00	0.00
2120-G	smokers	5	1.99	1.91	25.83	25.83
2121-A	smokers	7	0.18	0.52	2.91	2.35
2121-B	smokers	10	0.05	0.13	1.04	0.65
2121-C	smokers	9	0.02	0.13	0.55	0.31
2121-D	smokers	13	0.00	0.15	0.13	0.00
2121-E	smoker	8	0.11	0.30	3.22	1.37
2121-F	smoker	12	0.00	0.00	0.00	0.00

†lists the observed hydrothermal phenomena - all numbers presume the existance of a smoker.

Table 9. Vent Exit Conditions Based on Platinum Probe Data (Thermistor and Flowmeter)

Segment	Vent	Exit Temperature (°C)	Exit Velocity (m/s)	Location (x,y) (m)
Endeavor	2112-?	325	0.67	4994,6119
	2112-?	354	1.10	4992,6111
	2112-?	267	1.38	4945,6144
	2113-B	371†	-	4984,6159
		270	1.44	
	2113-R	374†	-	4984,6159
	2113-?	352†	-	5055,6200
	2113-T	342†	-	5045,6247
	2114-A	209	1.38	4937,6017
	2114-B	345	1.04	4884,5998
	2114-D	229	0.81	4886,6001
	2114-F	235	0.61	4920,6146
	2115-B	354†	-	5046,6242
		336	1.36	
		296	1.19	
	2115-C	296	1.21	5047,6246
		217	1.03	
		351†	-	
	2115-D	329†	-	5038,6248
		221	0.73	
	2115-H	217	1.12	4988,6180
	2115-J	333	0.56	4994,6182
	2116-D	237†	-	7046,7360
		239†	-	
	2116-?	227†	-	6886,7318
Southern	2117-C	222	0.67	11883,13197
	2117-C	229	0.91	11880,13195
	2117-H	292	0.82	11925,13225
	2118-?	25†	-	11254,11200
	2118-F	236†	-	11316,11366
	2118-G	303†	-	11317,11377
	2119-D	233†	-	12765,15613
	2119-E	271†	-	12710,15585
	2119-F	68	0.31	12706,15585
	2120-B	264†	-	11293,11328
	2120-B	174	0.43	11294,11328
	2120-?	69†	-	11315,11360
	2121-B	39†	-	11881,13207
	2121-D	350†	-	11943,13234
	2121-?	279†	-	11957,13284
	2121-?	290†	-	12154,14150
	2121-F	326†	-	12159,14118

† Data from the ALVIN high temperature probe.
? No correspondence to any other reported vent data in this paper.

Table 10. Compilation of Heat Flux Estimates

Vent Label†	min H_T	max H_T	min H_V	max H_V	Sample List
2112-E	1.5	6.6	1.0	13.2	2112-E,F
2112-K	4.7	15.8	1.9	40.4	2112-K
2113-B	16.2	49.6	2.1	30.0	2113-B††,R
2113-E	8.2	24.6	2.7	35.3	2113-E
2113-Q	4.9	14.2	0.5	6.5	2113-Q
2113-S	4.6	14.3	2.6	33.7	2113-S;2115-B††
2115-Q	1.3	4.3	0.0	1.4	2113-T††;2115-C,D,Q
2115-F	1.4	4.0	0.9	11.2	2115-D††,F
2114-T	5.5	16.2	0.1	1.6	2114-A††,T
2114-S	1.4	3.9	0.0	0.1	2114-Q,S
2114-F	3.4	12.2	0.4	7.3	2114-F††
2114-V	0.1	0.8	0.0	0.8	2114-V
2114-B	0.8	5.8	0.3	4.3	2114-B††,C1,C2,D
2114-C3	0.6	2.9	0.0	0.1	2114-C3,C4
2115-A	1.8	6.6	0.0	0.1	2115-A
2115-J	6.8	33.9	4.5	74.8	2115-H,J
2116-D	0.8	2.9	0.0	0.2	2116-D††
2116-G	6.2	20.2	1.3	30.7	2116-G
2117-A	0.1	2.9	-	-	2117-A
2117-B	0.0	4.3	-	-	2117-B
2121-C	1.0	4.3	0.0	0.6	2121-C
2121-B	6.3	18.3	0.1	1.0	2117-C††;2121-A,B
2117-E	0.6	2.3	0.0†††	0.2†††	2117-D,E,F,G;2121-D
2117-H	0.4	1.4	-	-	2117-H††,I,J
2117-K	0.0	2.5	-	-	2117-K
2121-E	2.1	8.0	0.1	3.2	2121-E
2121-F	1.4	4.2	0.0	0.0	2121-F
2118-D	0.1	1.1	0.0	0.3	2118-D,E
2120-F	0.2	3.3	0.0	0.0	2118-F,G,H;2120-D,E,F
2120-A	0.0	0.4	0.0	0.0	2120-A
2120-B	2.1	6.0	0.0	0.4	2120-B††
2120-C	0.7	3.0	0.0	0.6	2120-C
2120-G	0.2	0.5	2.0	25.8	2120-G
2119-A	0.2	1.0	0.0	0.1	2119-A,B
2119-C	0.2	0.6	0.0	0.0	2119-C,D
2119-F	0.1	1.4	0.0	0.0	2119-E,F††

† Representing sample - chosen to yield the largest value of minimum estimate of heat flux based on the array temperature data.
†† Indicates sample during which vent exit parameters were measured.
††† From 2121-D.

Table 11. Crustal Accretion - Geothermal Heat Flux Model Estimates

Model	Heat Flux per meter Ridge (MW/m)	Reference
heat sink:		
- max hydrothermal output	10000 W per m ridge	Morton and Sleep, 1985
- heat sink total	8400 W per m ridge	
- conductive heat flux	1800 W per m ridge	
magma chamber	6 MW for 1 km^3 magma	†
cracking hot rock	280 to 24000 W/m^2	Lister, 1983
slab of new crust	8100 W per m ridge	†

† calculated in text.

Table 12. Comparison of theoretical and observed heat flux estimates.

	Endeavor Segment	Southern Segement
# of vent samples	31	35
# of unique vents	18	18
estimated segment length	110 km	70 km
OBSERVED HEAT FLUX:		
this study, minimum	70 MW	16 MW
this study, maximum	236 MW	66 MW
Baker and Massoth, 1987	1700 ± 1100 MW	580 ± 351 MW
THEORETICAL HEAT FLUX:		
heat flow anomaly	4300 MW	2700 MW
crustal accreation (slab model)	900 MW	570 MW
magmatic crystallization	6 MW per 1 km^3 magma crystallized in 5000 yrs	

Table 13. Average heat flux and radial distance† esimates for selected hydrothermal vents compared with estimates from Table 10.

Vent	r†† (m)	H†† (MW)	Hmin (MW)	Hmax (MW)
2112-E	2.40 ± 0.76	3.1 ± 1.7	1.0	6.6
2113-B	1.59 ± 0.81	17.5 ± 6.7	16.2	49.6
2113-E	2.20 ± 0.90	9.8 ± 4.0	8.2	24.6
2113-S	2.99 ± 1.78	5.4 ± 3.3	4.6	14.3
2114-F	2.40 ± 0.84	5.4 ± 1.9	3.4	12.2
2115-D	1.66 ± 1.04	3.2 ± 1.2	1.2	7.9
2115-F	1.60 ± 1.15	2.1 ± 1.1	1.4	4.0
2115-J	1.62 ± 0.39	13.1 ± 2.2	6.9	33.9
2116-D	4.46 ± 2.12	4.9 ± 4.3	0.8	2.9

† distance between the array (instrument measuring temperature) and the plume centerline.

†† Calculations based on the mean temperature T_{hot} reported in Table 5. Four pairs of thermistors are used in the averages; calulations which result in an imaginary radial distance are dropped.

Table 14. Calibration Equations and Constants

Frequency F to Resistance R: $R = A + BF + CF^2 + DF^3$

Thermistor	A	B	C ($\times 10^{-7}$)	D ($\times 10^{-11}$)
T1	5205.2	-0.16721	4.3439	0
T2	5171.3	-0.15051	-6.1252	2
T3	5176.4	-0.13463	-1.7431	4
T4	5202.3	-0.16314	0.1550	1
T5	5161.3	-0.13643	-8.8339	1
Platinum	249.25	-0.0034	-0.002	0

Resistance R to Temperature T: $T = 1/(A + B\ln R + C(\ln R)^3)$

Thermistor	A ($\times 10^{-2}$)	B ($\times 10^{-3}$)	C ($\times 10^{-5}$)
T1	0.129314482	0.265097611	0.153157863
T2	0.130389364	0.265555570	0.145066946
T3	0.129706906	0.264198762	0.153818400
T4	0.130435167	0.262647541	0.151624783
T5	0.131801772	0.261478963	0.140212015

Platinum $T = -244.04 + 2.3318R + 0.0001R^2$

Figure 1. Location of the Endeavor and Southern Segments along the Juan de Fuca Ridge. After Baker and Massoth [1997] and Karsten et al. [1990].

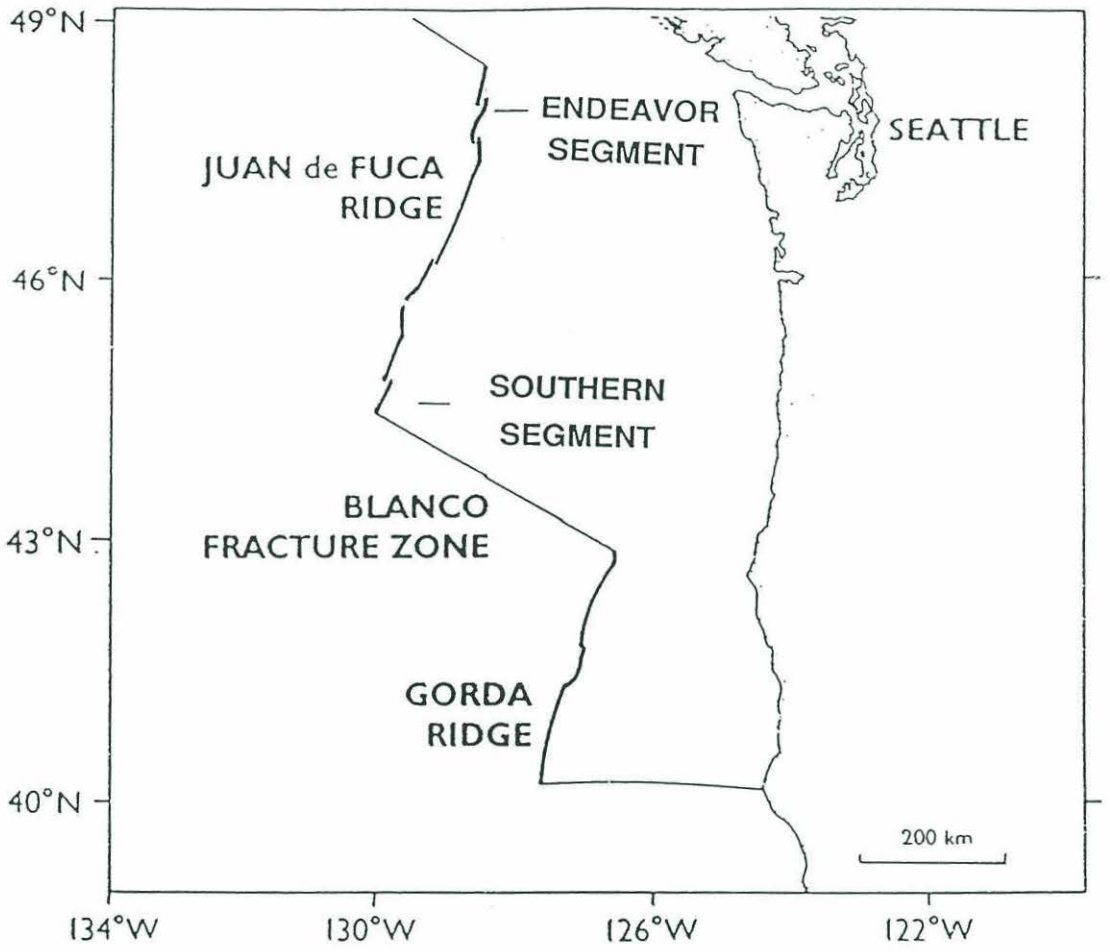
49°N
46°N
43°N
40°N
134°W
130°W
126°W
122°W
ENDEAVOR SEGMENT
JUAN de FUCA RIDGE
SEATTLE
SOUTHERN SEGMENT
BLANCO FRACTURE ZONE
GORDA RIDGE
200 km

Figure 1

Figure 2. Location of vents visited in the Endeavor Segment of the Juan de Fuca Ridge. Symbols distinguish between the five dives. (a) Dives 2112 - 2115. Map courtesy of Delaney. (b) Dive 2116. (c) Dives 2117-2121.

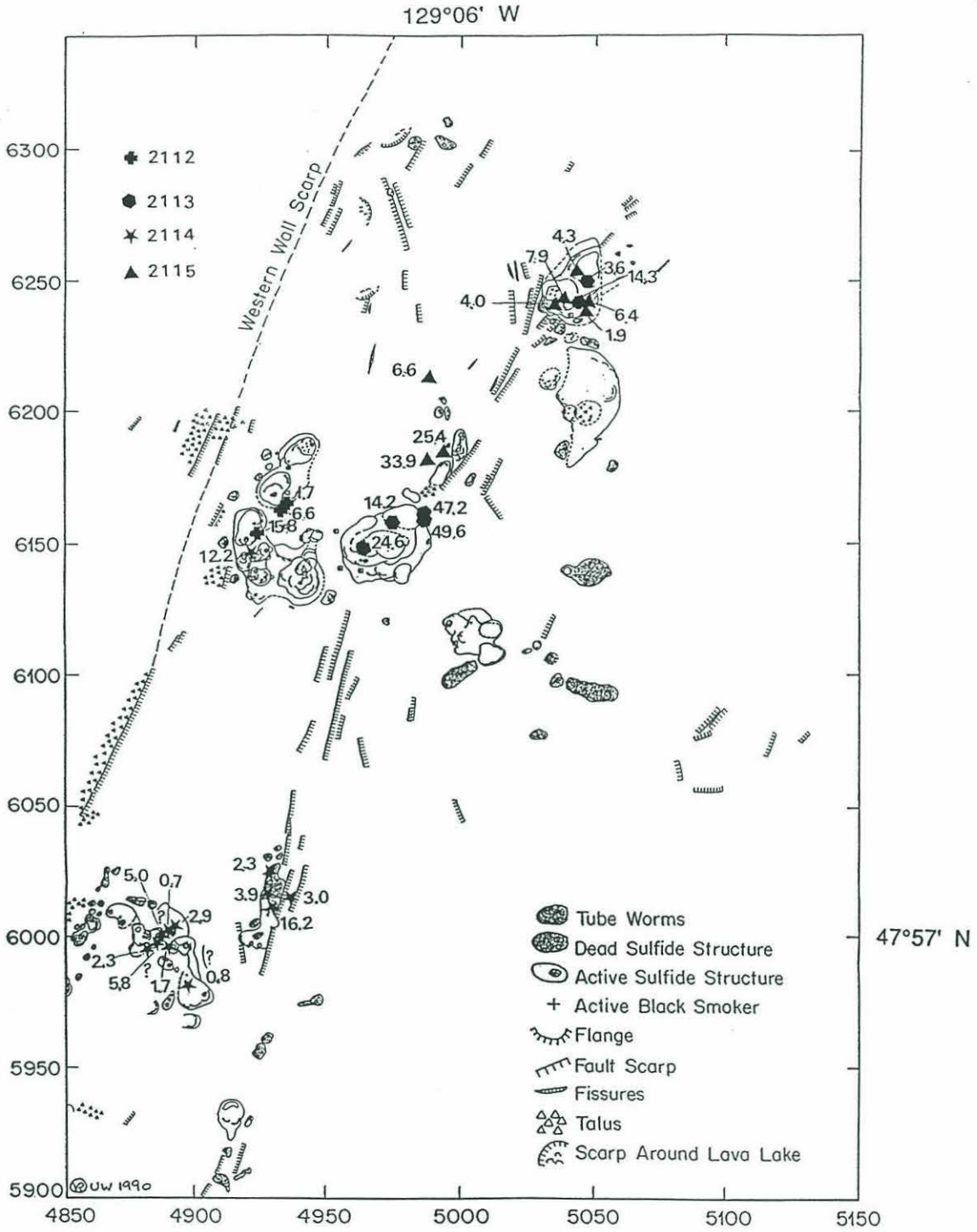
129°06' W
47°57' N
2112
2113
2114
2115
Western Wall Scarp
6300
6250
6200
6150
6100
6050
6000
5950
5900
4850
4900
4950
5000
5050
5100
5150
4.3
7.9
3.6
14.3
4.0
6.4
1.9
6.6
25.4
33.9
14.2
47.2
49.6
24.6
1.7
6.6
15.8
12.2
5.0
0.7
2.9
2.3
5.8
1.7
0.8
2.3
3.9
3.0
16.2
Tube Worms
Dead Sulfide Structure
Active Sulfide Structure
Active Black Smoker
Flange
Fault Scarp
Fissures
Talus
Scarp Around Lava Lake
UW 1990

Figure 2a

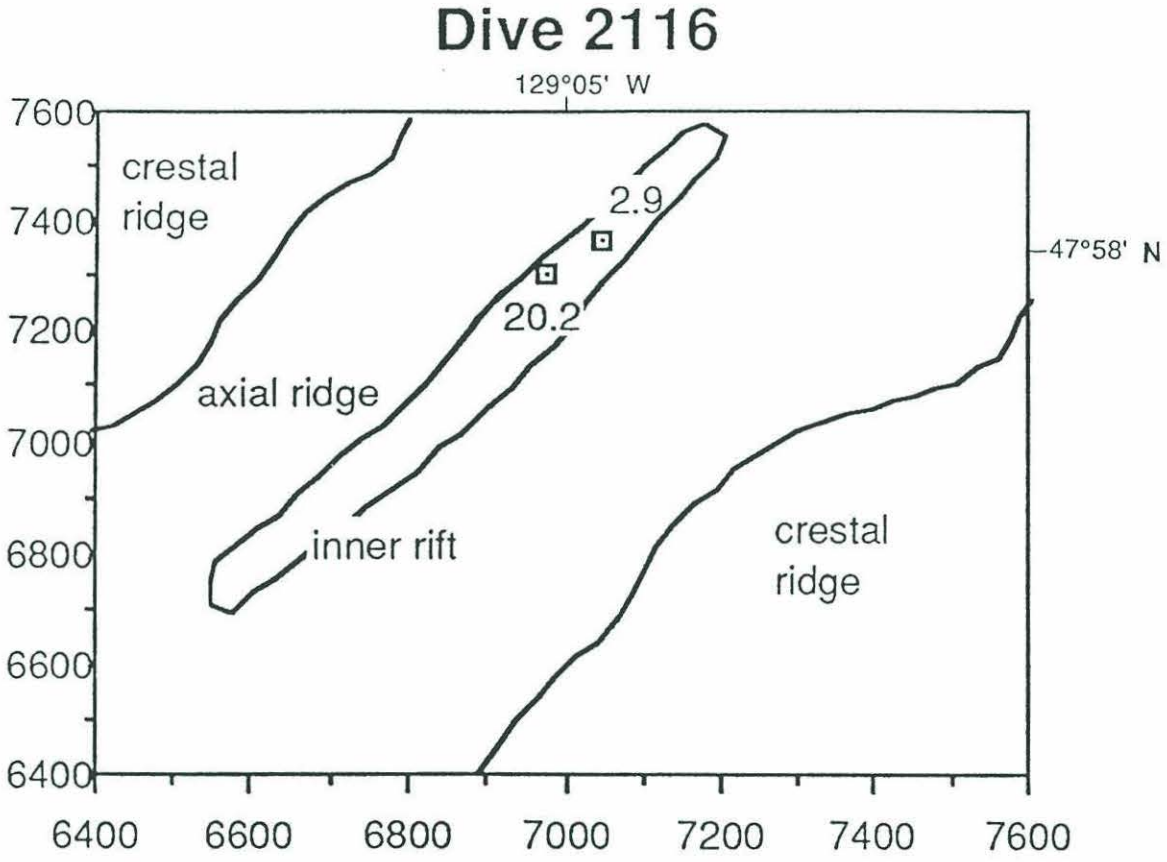
Dive 2116
129°05' W
47°58' N
crestal ridge
axial ridge
inner rift
crestal ridge
2.9
20.2
7600
7400
7200
7000
6800
6600
6400
6400
6600
6800
7000
7200
7400
7600

Figure 2b

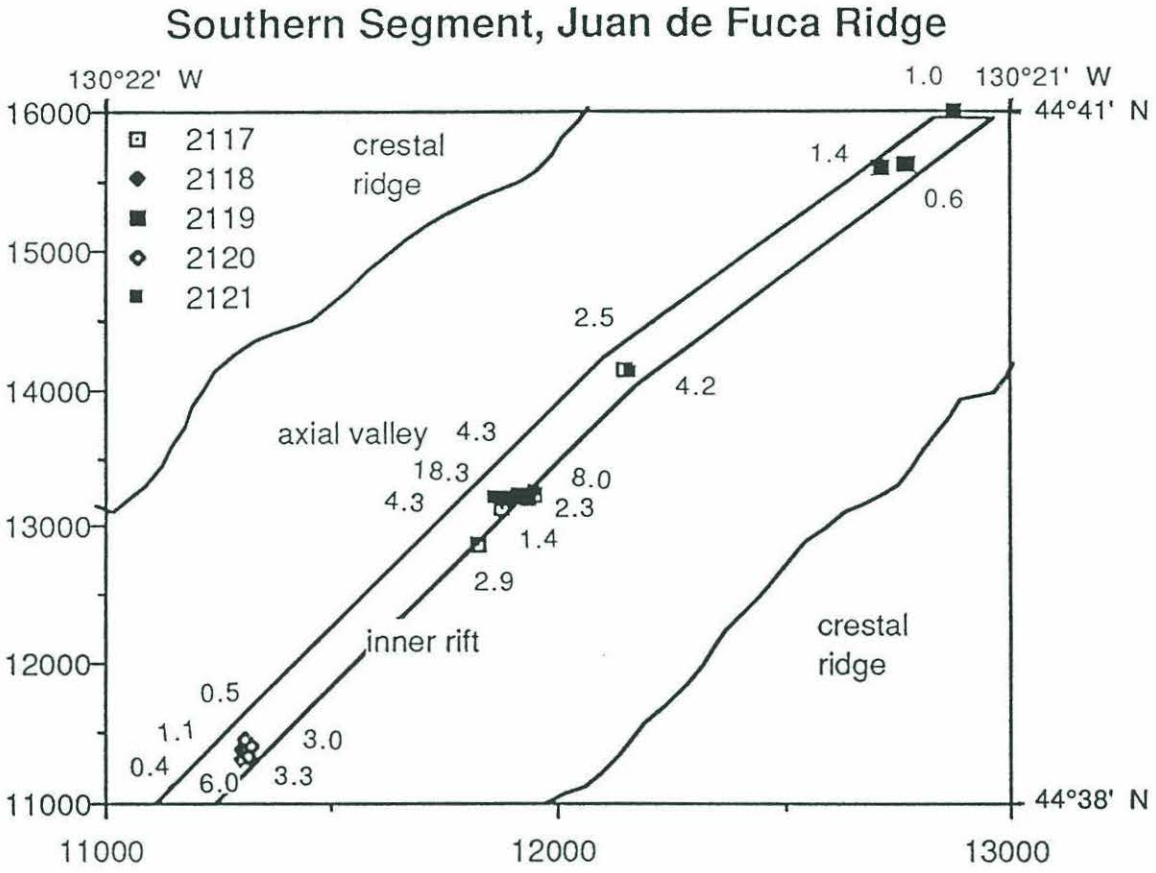
Southern Segment, Juan de Fuca Ridge
130°22' W
1.0
130°21' W
44°41' N
44°38' N
16000
15000
14000
13000
12000
11000
11000
12000
13000
2117
2118
2119
2120
2121
crestal ridge
axial valley
inner rift
crestal ridge
1.4
0.6
2.5
4.2
4.3
18.3
4.3
8.0
2.3
1.4
2.9
0.5
1.1
0.4
6.0
3.3
3.0

Figure 2c

Figure 3. Diagram of the thermistor array attached to D/V ALVIN.

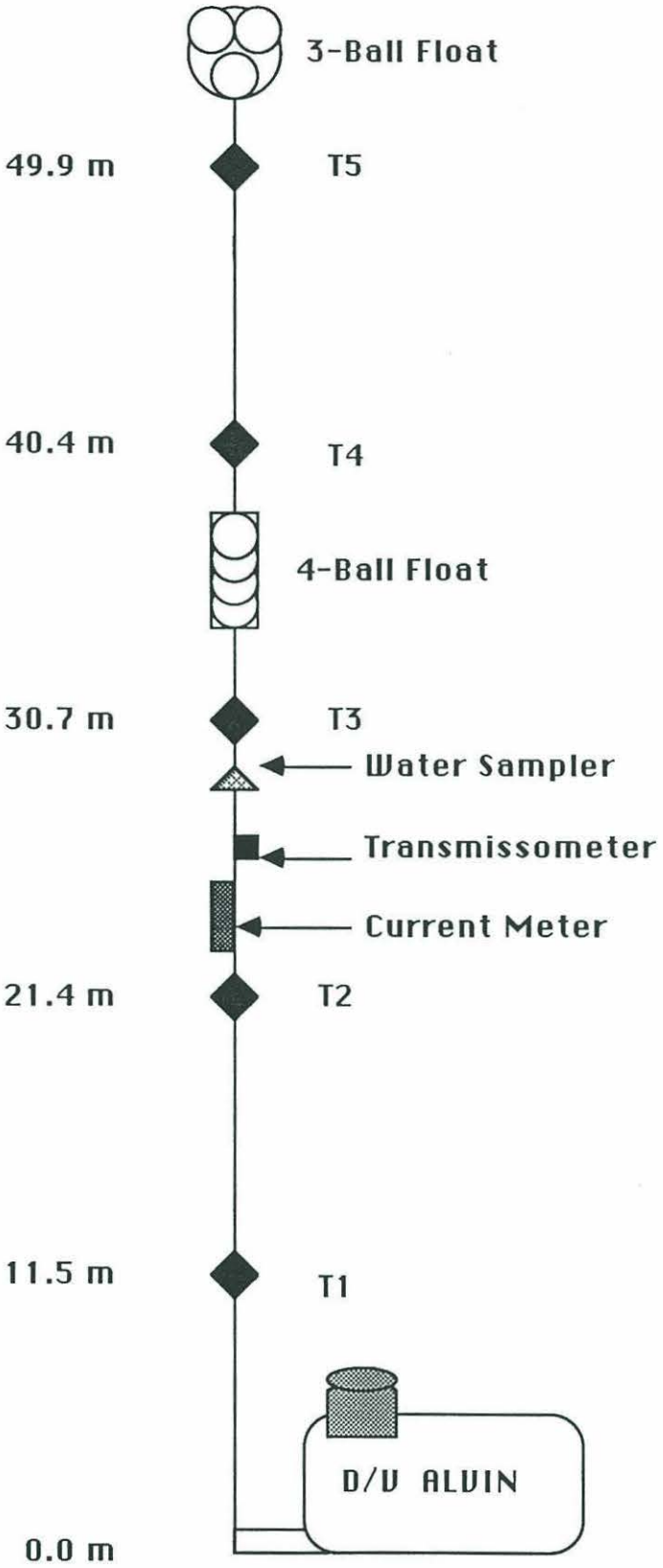
3-Ball Float
49.9 m
T5
40.4 m
T4
4-Ball Float
30.7 m
T3
Water Sampler
Transmissometer
Current Meter
21.4 m
T2
11.5 m
T1
D/V ALVIN
0.0 m

Figure 3.

Figure 4. Temperature and velocity profiles for dive 2113. Sections where ALVIN was stationary are marked by short black lines between the profiles from thermistors T5 and T4. All profiles are offset from zero by a constant amount.

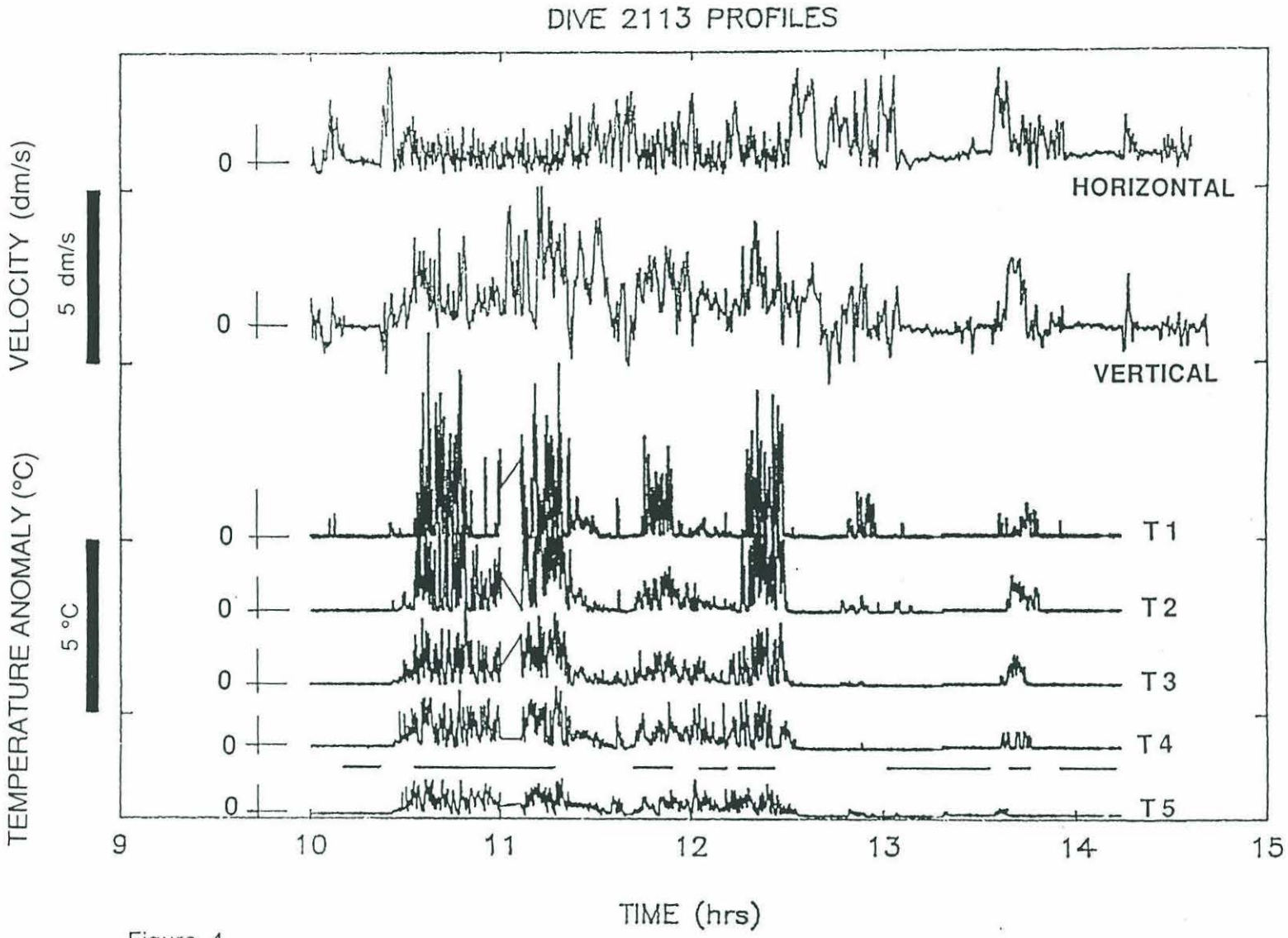
DIVE 2113 PROFILES
VELOCITY (dm/s)
5 dm/s
HORIZONTAL
VERTICAL
TEMPERATURE ANOMALY (°C)
5 °C
T1
T2
T3
T4
T5
0
9
10
11
12
13
14
15
TIME (hrs)

Figure 4

Figure 5. A diagram of a plume in a stratified environment.

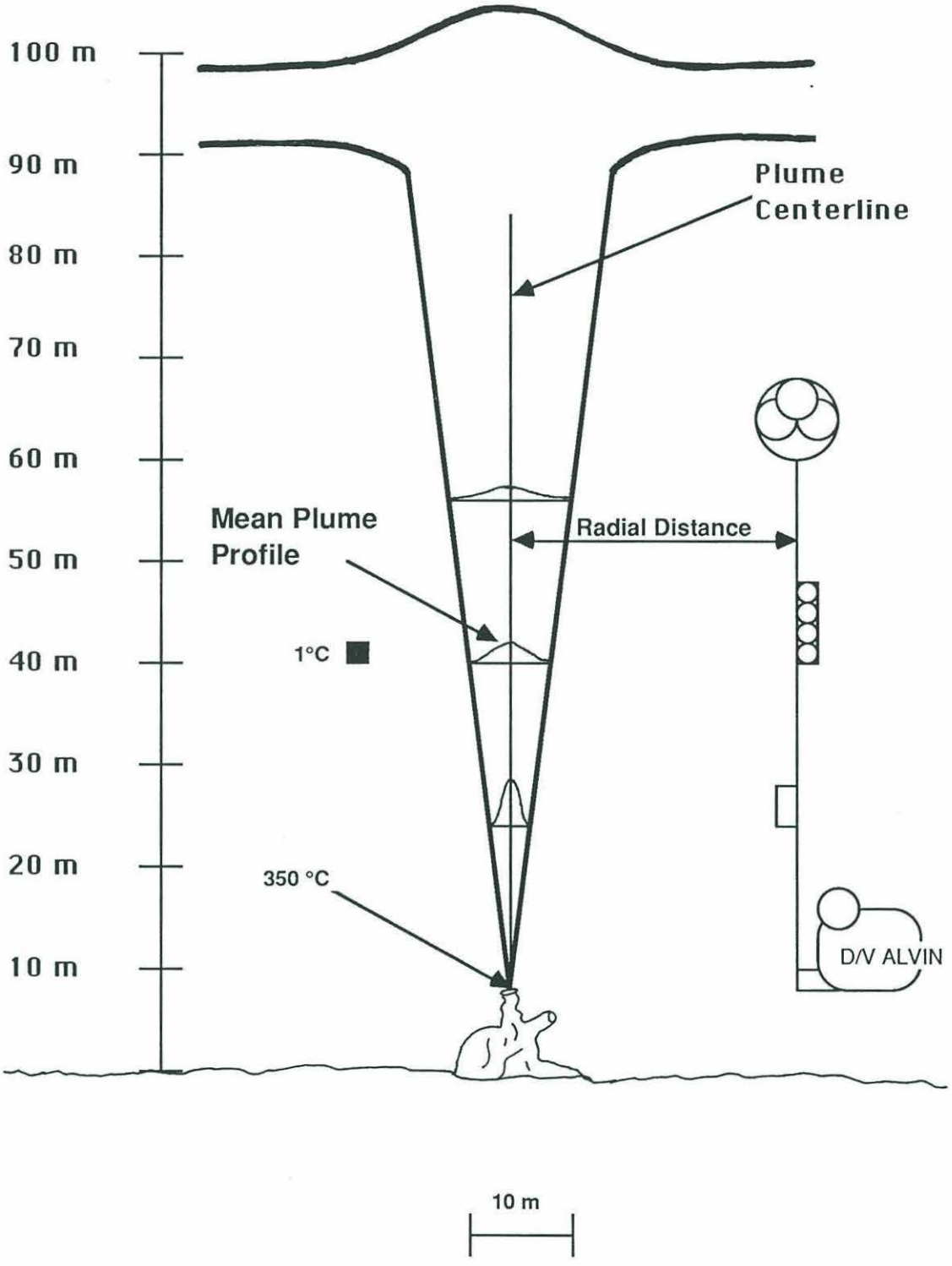
100 m
90 m
80 m
70 m
60 m
50 m
40 m
30 m
20 m
10 m
Plume
Centerline
Mean Plume
Profile
Radial Distance
1°C
350 °C
D/V ALVIN
10 m

Figure 5

Figure 6. Time series of velocity and temperature measured at vent 2113-E. Temperature profiles are progressively offset by 2°C.

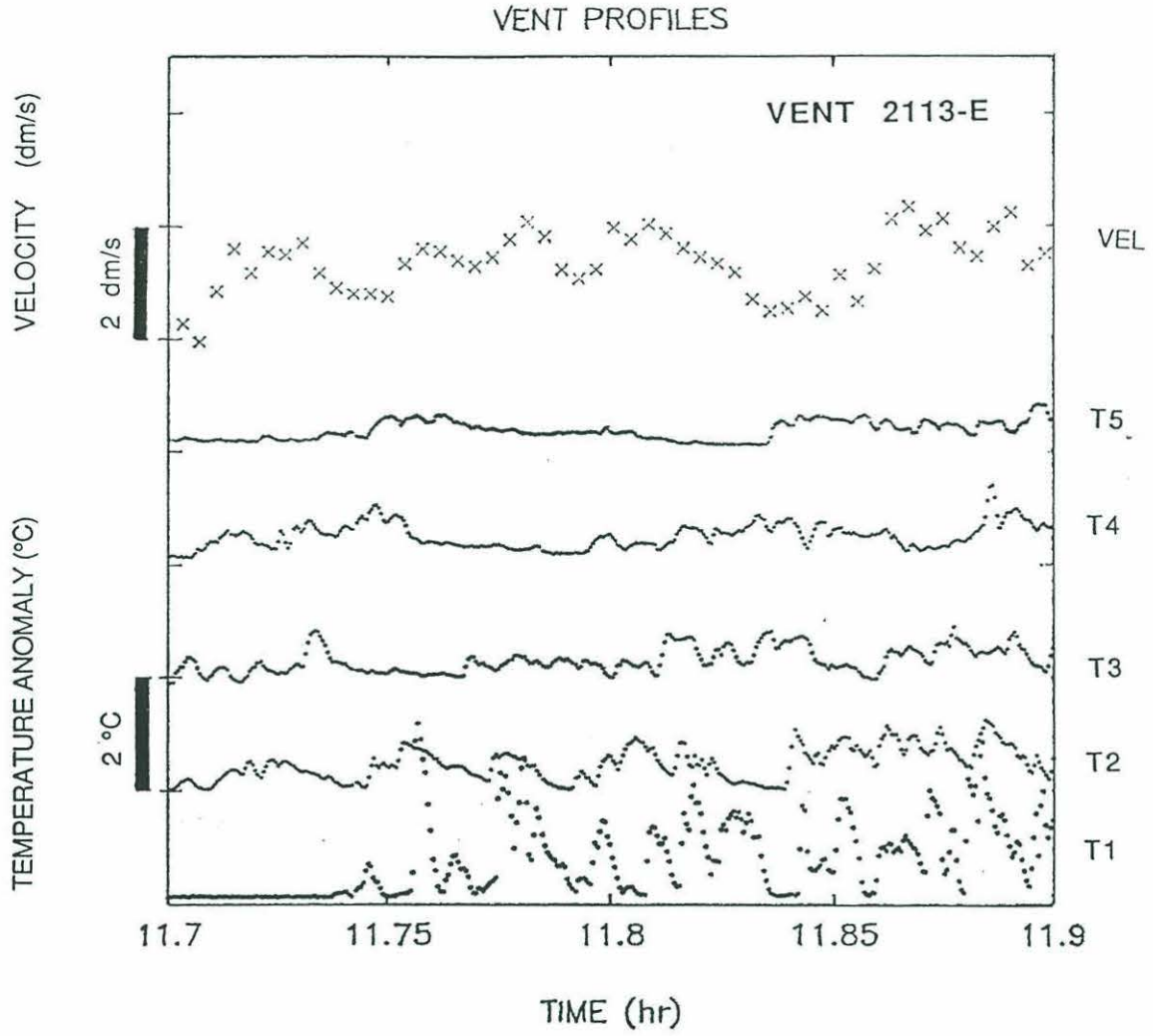
VENT PROFILES
VENT 2113-E
VELOCITY (dm/s)
2 dm/s
VEL
T5
T4
T3
T2
T1
TEMPERATURE ANOMALY (°C)
2 °C
11.7
11.75
11.8
11.85
11.9
TIME (hr)

Figure 6

Figure 7. Mean centerline temperature anomaly estimates v.s. height for vent 2113-E. Estimates are based on the maximum (T_{max} - x) and mean (T_{cold}, T_{hot} - o) observed temperature. Solid curves are lines of constant heat flux given by equation (2). Mean centerline temperature estimated from the radial distance from the plume centerline (T(r) - *) as given in Appendix I.

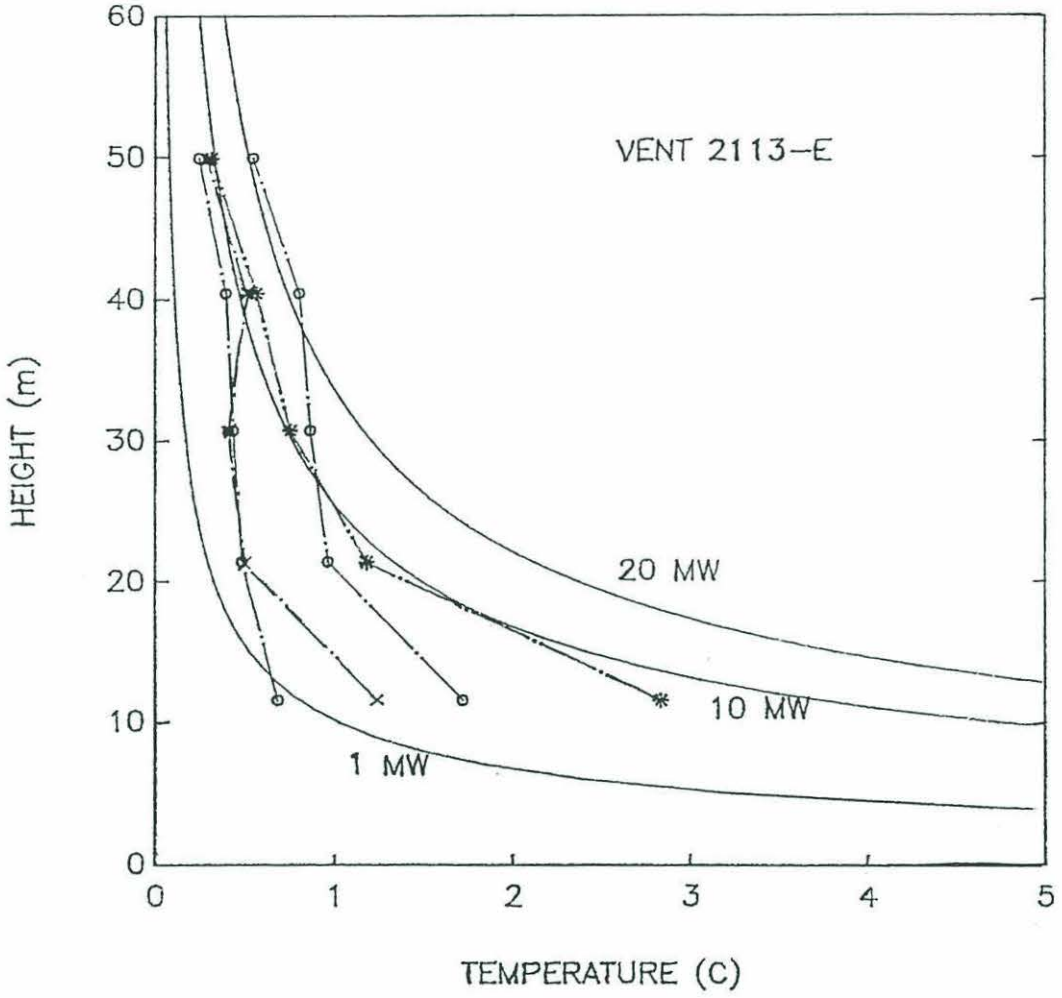
VENT 2113-E
20 MW
10 MW
1 MW
HEIGHT (m)
TEMPERATURE (C)
0
10
20
30
40
50
60
0
1
2
3
4
5

Figure 7

Figure 8. Mean centerline velocity estimates v.s. height. Curves of constant heat flux are given by equation (1). Symbols as in Figure 7.

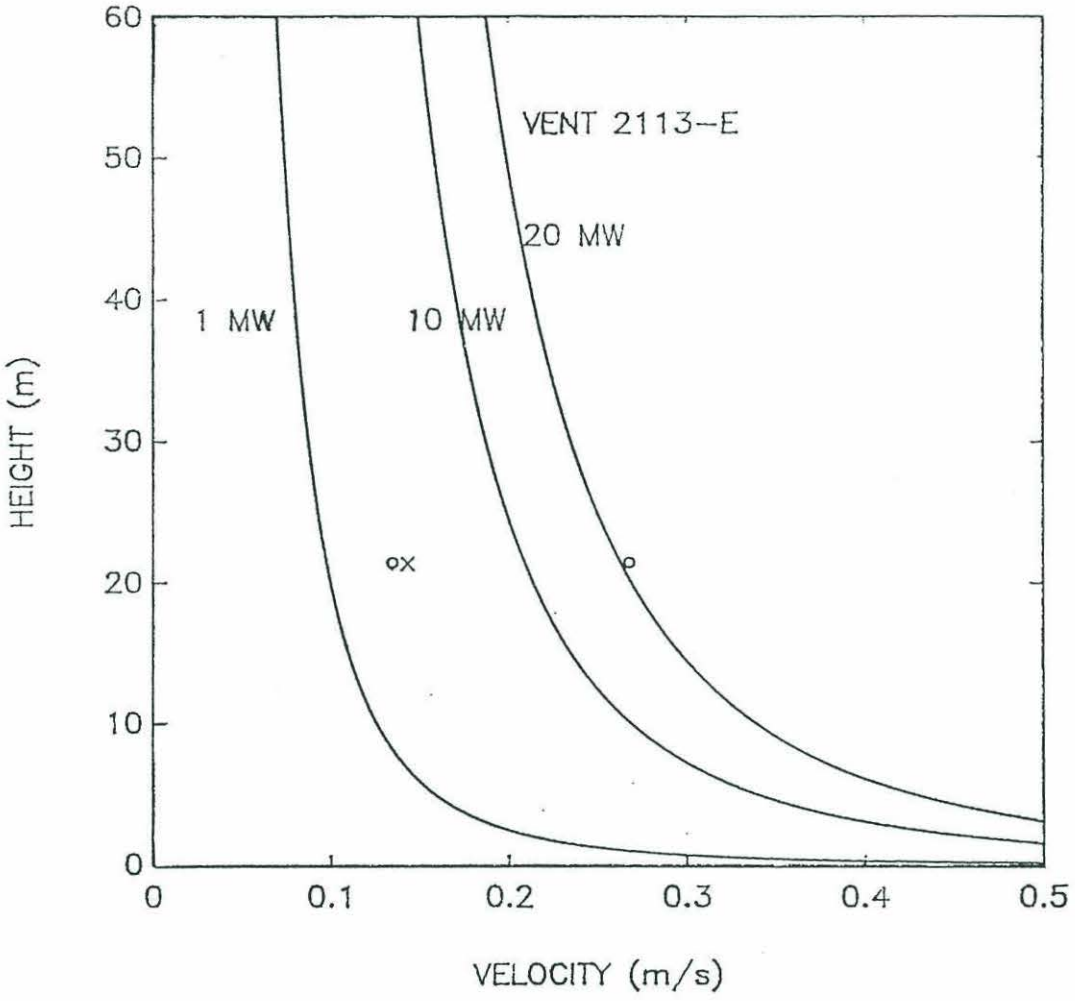
VENT 2113-E
20 MW
10 MW
1 MW
HEIGHT (m)
VELOCITY (m/s)
60
50
40
30
20
10
0
0
0.1
0.2
0.3
0.4
0.5

Figure 8

Figure 9. Laboratory data showing the relationship of the maximum and mean centerline values for a number of runs. (a) velocity. (b) tracer concentration. From Papanicolaou and List [1988].

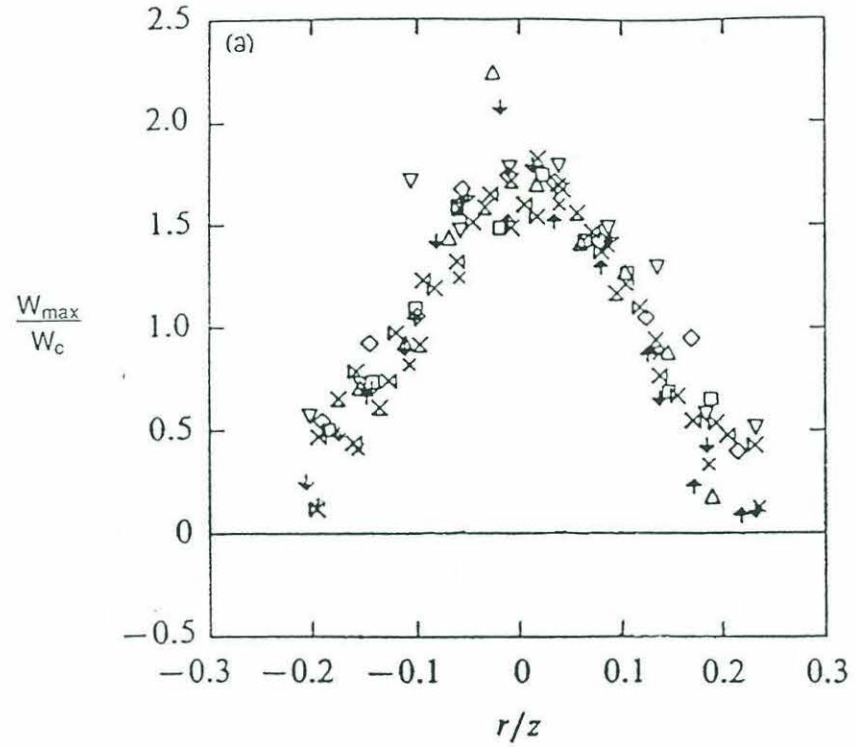
(a)
2.5
2.0
1.5
1.0
0.5
0
−0.5
−0.3
−0.2
−0.1
0
0.1
0.2
0.3
$\frac{W_{max}}{W_c}$
r/z

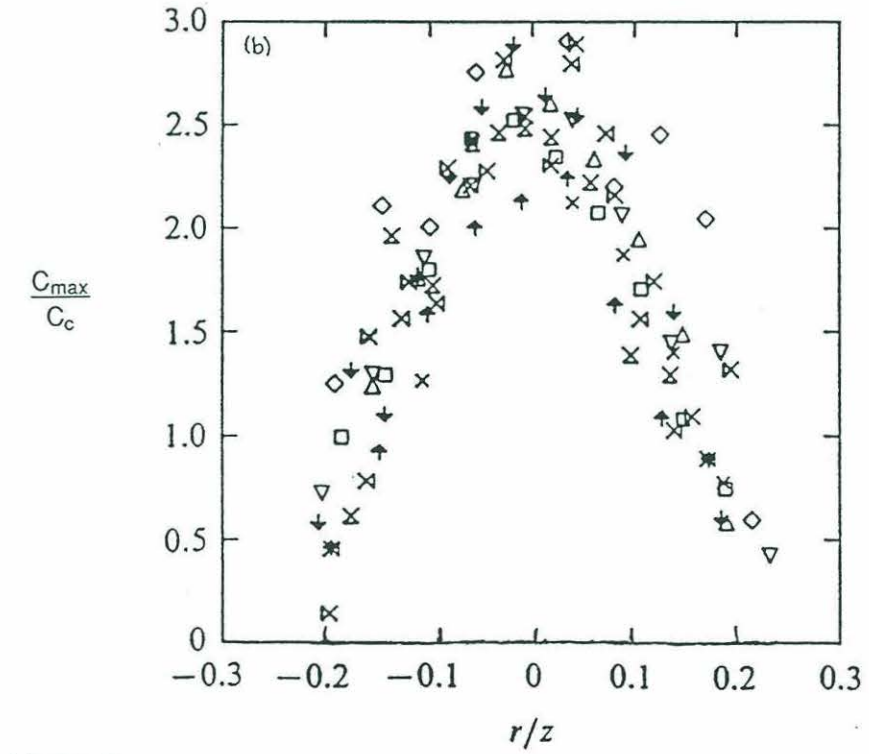
(b)
3.0
2.5
2.0
1.5
1.0
0.5
0
−0.3
−0.2
−0.1
0
0.1
0.2
0.3
$\frac{C_{max}}{C_c}$
r/z

Figure 9

Figure 10. A comparison of an ideal guassian profile to observed time-averaged profiles of a plume (laboratory data from Papanicolaou and List [1987]) illustrates the relationship of the time-averaged temperature profile with the flow-weighted average temperature.

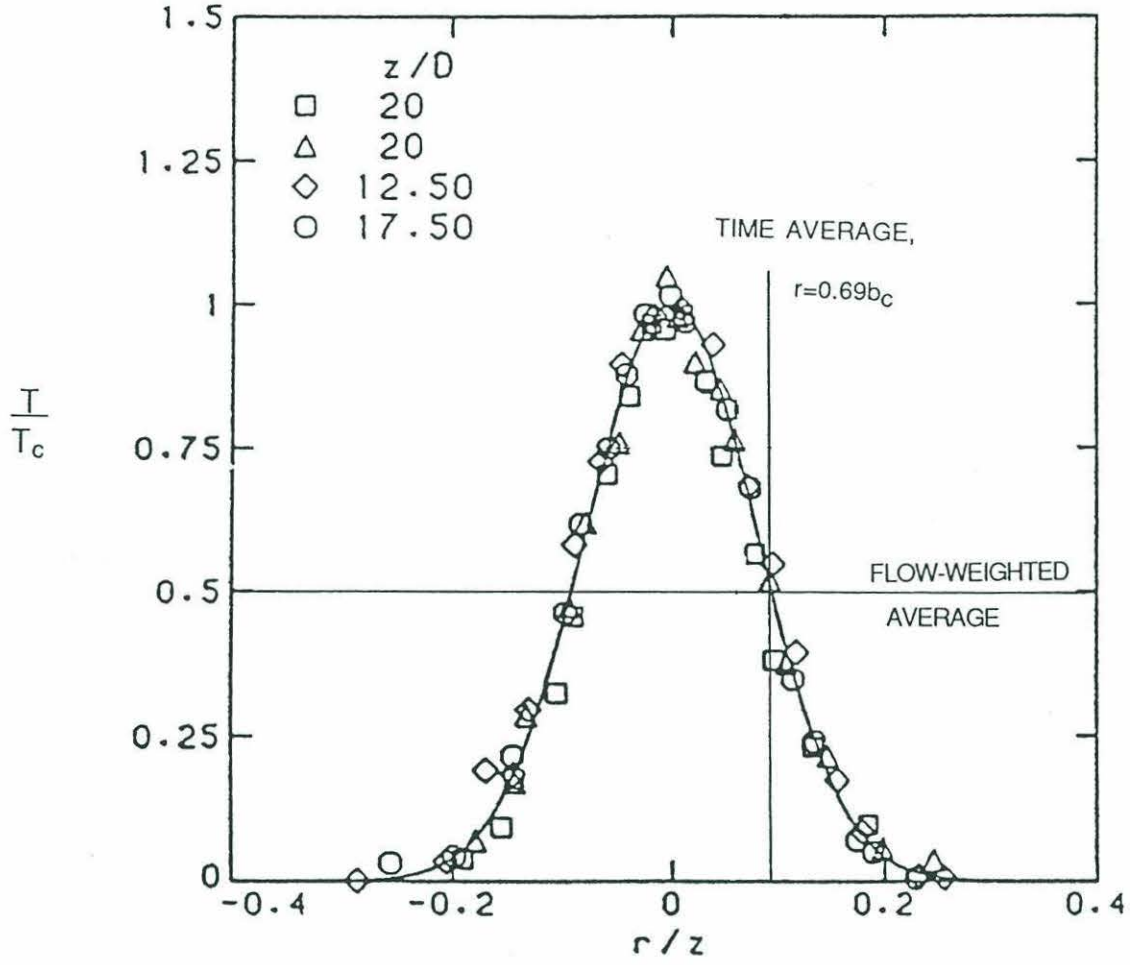
1.5
1.25
1
0.75
0.5
0.25
0
z/D
20
20
12.50
17.50
TIME AVERAGE,
r=0.69b_c
FLOW-WEIGHTED
AVERAGE
T/T_c
-0.4
-0.2
0
0.2
0.4
r/z

Figure 10

Figure 11. A comparison of time-averaged laboratory data and an ideal guassian profile for velocity [Papanicolaou and List, 1988] illustrates the relationship between the average value of a guassian profile of half-width b_w and the centerline value of the same profile.

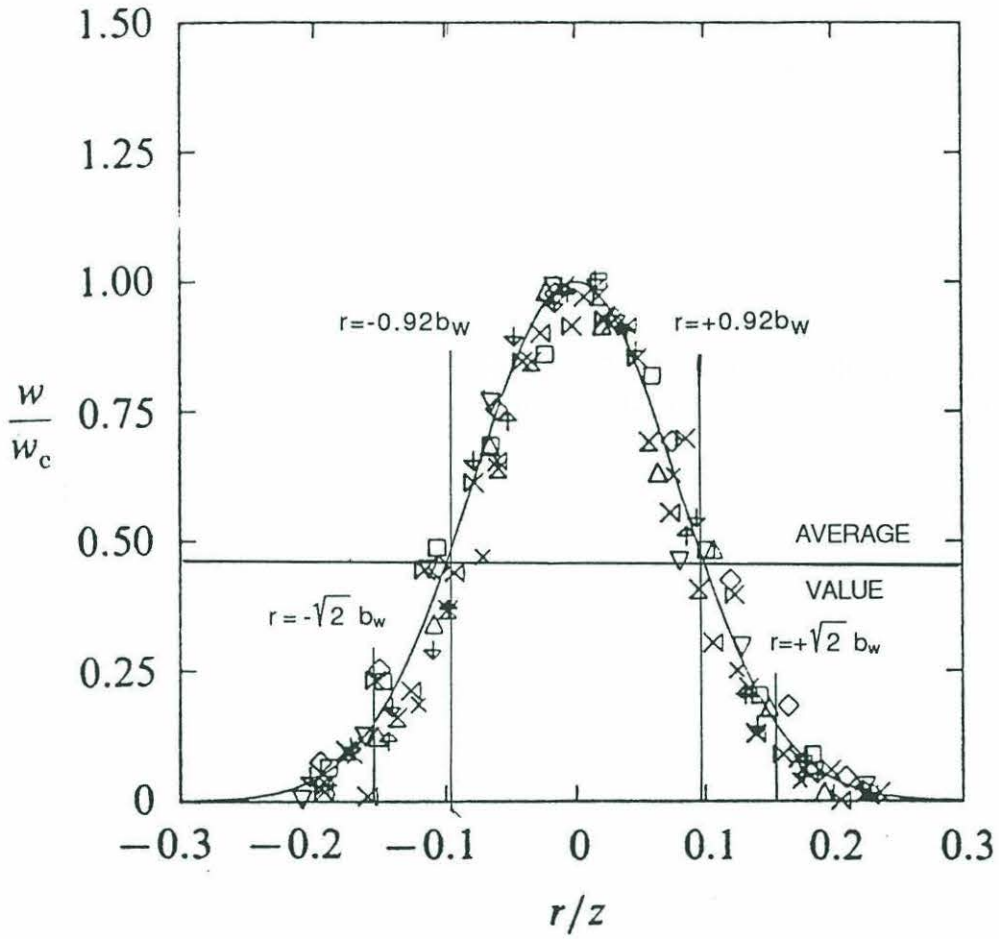
1.50
1.25
1.00
0.75
0.50
0.25
0
w/w_c
r=-0.92b_w
r=+0.92b_w
AVERAGE
VALUE
r=-√2 b_w
r=+√2 b_w
−0.3
−0.2
−0.1
0
0.1
0.2
0.3
r/z

Figure 11

Figure 12. A plume in a crossflow of velocity U. z_B is the height at which the crossflow begins to dominate the plume behavior.

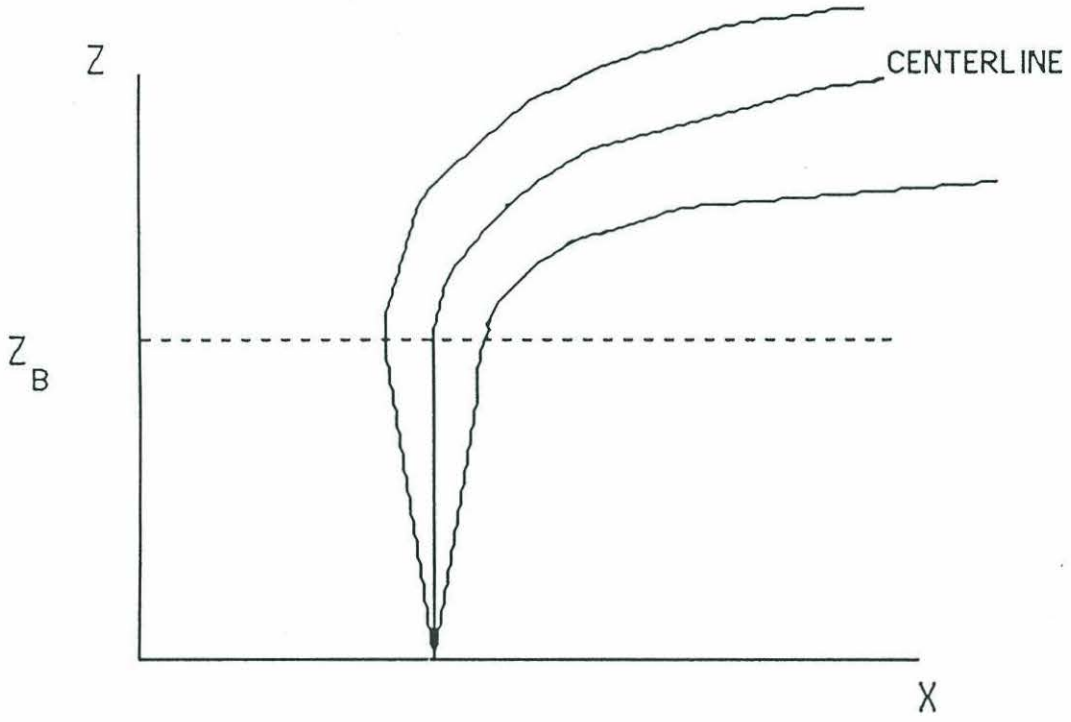

Figure 12

Figure 13. Two perpendicular horizontal velocity components plotted against each other to show that the mean horizontal velocity is zero at z=~20 m in this location. This is the same time section (vent 2113-E) as used in Figures 4 - 7. The distribution of velocity vector endpoints (o) is random in time.

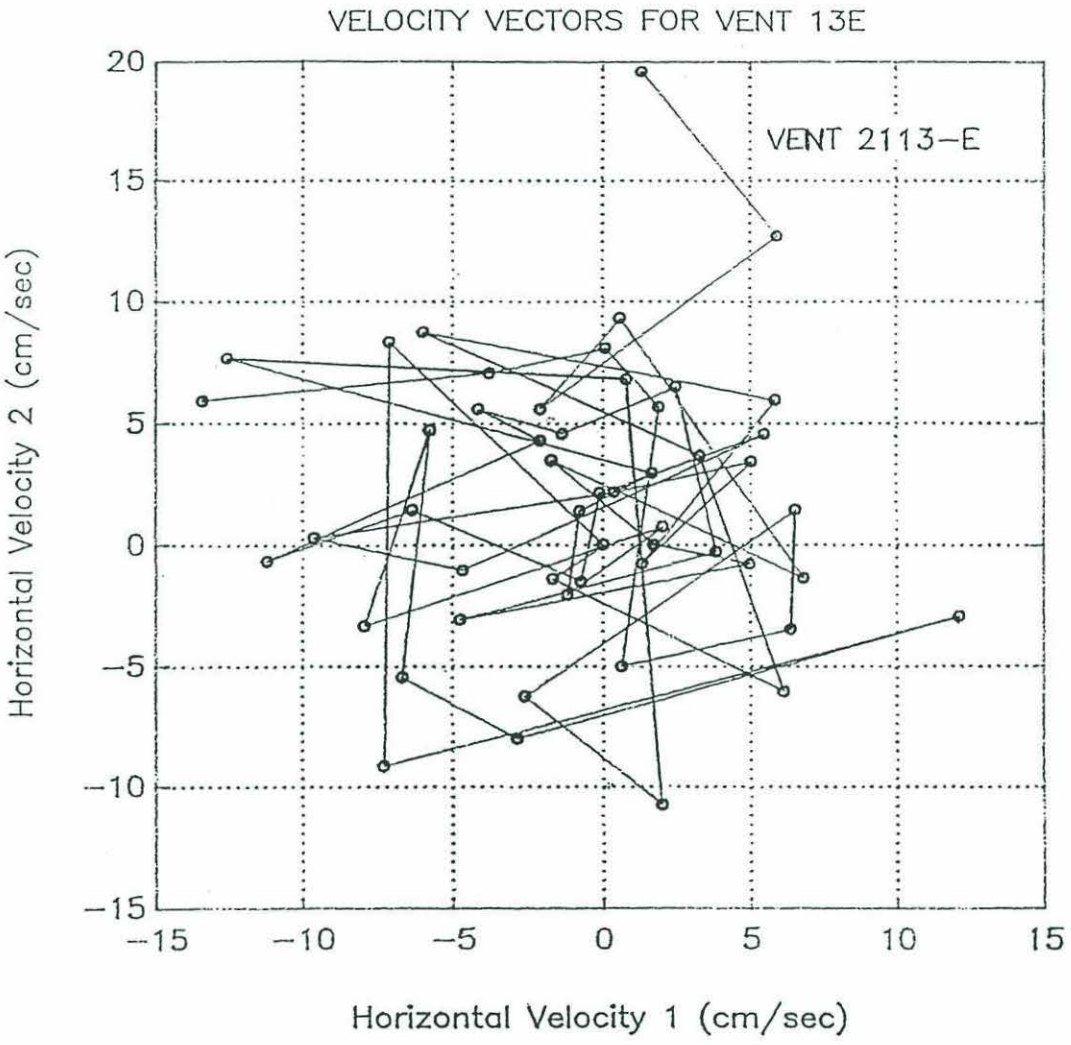
VELOCITY VECTORS FOR VENT 13E
VENT 2113-E
Horizontal Velocity 2 (cm/sec)
Horizontal Velocity 1 (cm/sec)
20
15
10
5
0
-5
-10
-15
-15
-10
-5
0
5
10
15

Figure 13

Figure 14. Accretion of new crust as a slab. Quantities used in the discussion in the text of the resultant heat flux are indicated.

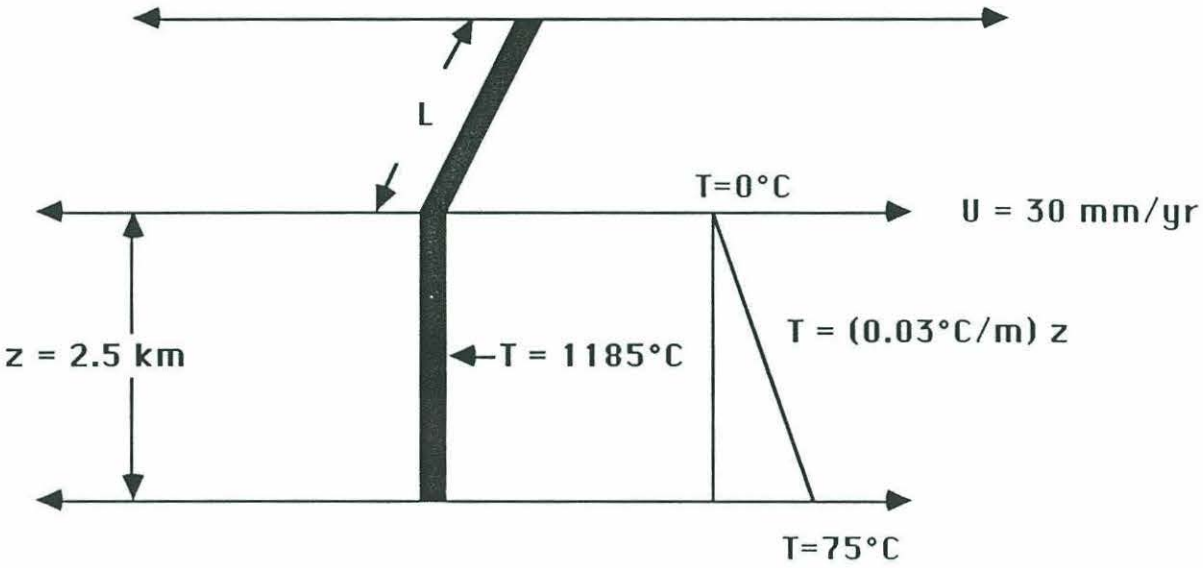

Figure 14.

Figure 15. Mean centerline temperature and heat flux estimated as a function of the radial distance between the plume centerline and the array (Solid boxes). Solid curves show the estimates based on an assumed radius (Table 10) and T_{cold} (solid diamonds), T_{hot} (open boxes) or T_{max} (open diamonds).

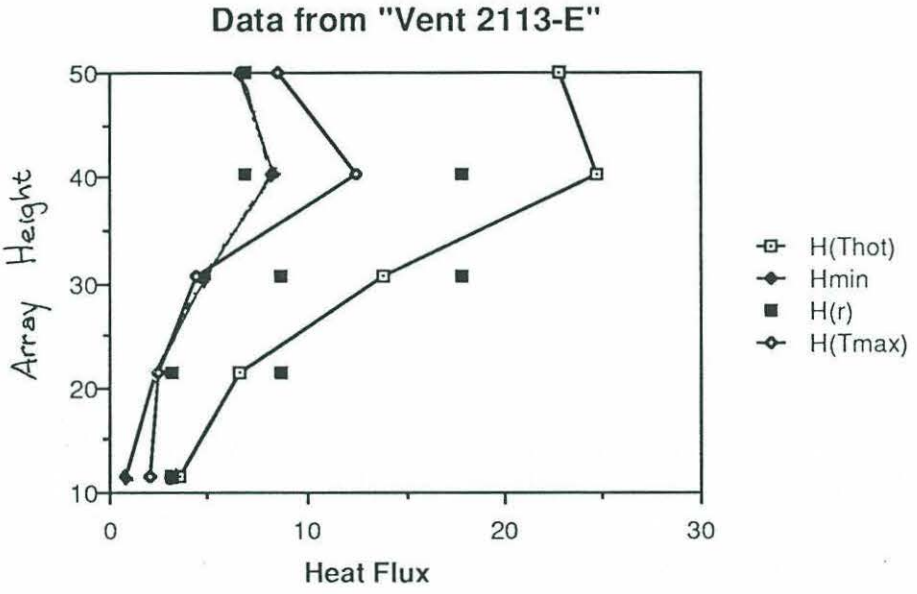
Data from "Vent 2113-E"
Array Height
50
40
30
20
10
0
10
20
30
Heat Flux
H(Thot)
Hmin
H(r)
H(Tmax)

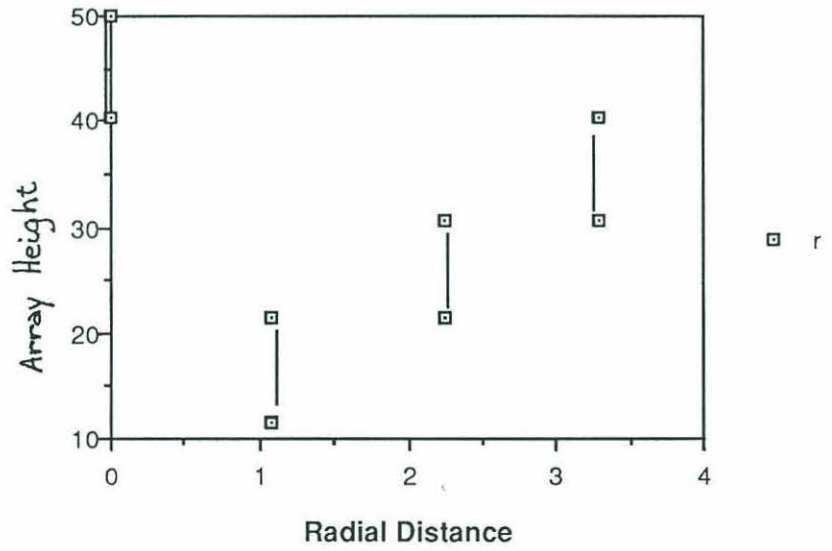
Array Height
50
40
30
20
10
0
1
2
3
4
Radial Distance
r

Figure 15

Figure 16. Conductive heat flow data (solid circles) [from Moran and Lister, 1987] compared to the theoretical predictions of the half-space cooling model (solid line). The heat flow anomaly for the Juan de Fuca Ridge depends on the difference (dashed line).

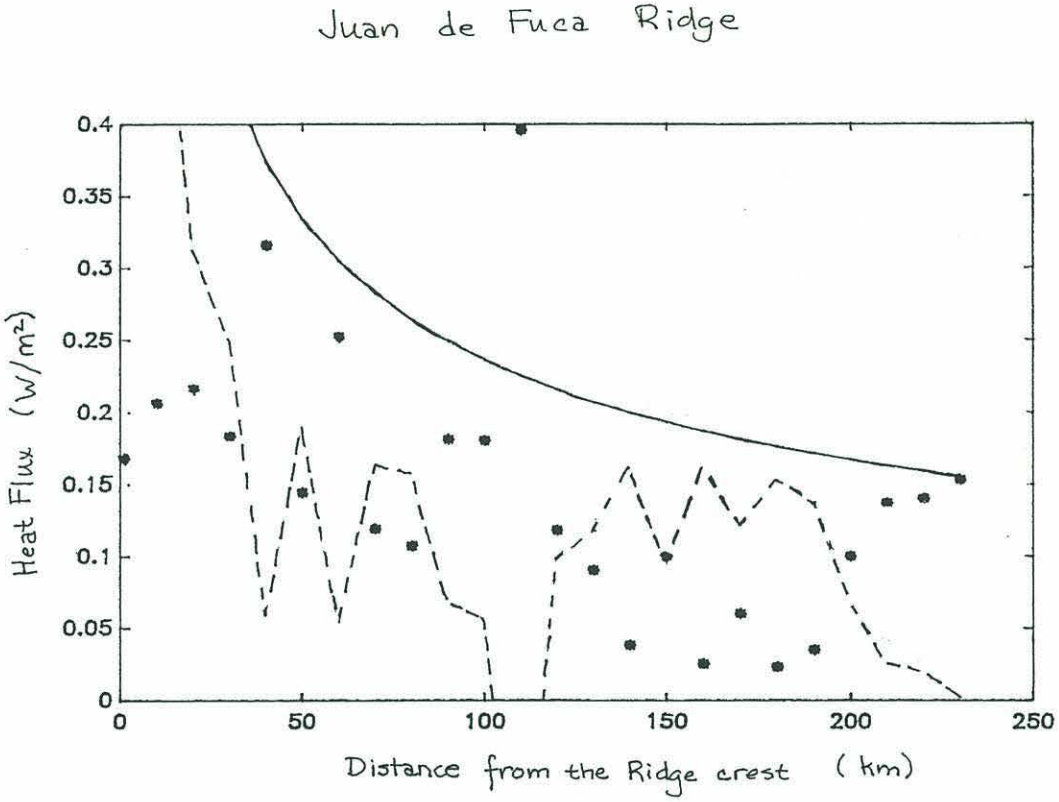
Juan de Fuca Ridge
Heat Flux (W/m²)
0.4
0.35
0.3
0.25
0.2
0.15
0.1
0.05
0
0
50
100
150
200
250
Distance from the Ridge crest (km)

Figure 16

References

Alt, J. C., J. Honnorez, C. Laverne, and R. Emmermann. Hydrothermal alteration of a 1 km section through the upper oceanic crust, Deep Sea Drilling Project Hole 504B: Mineralogy, chemistry, and evolution of the seawater-basalt interaction. Journal of Geophysical Research, vol. 91 (B10), pp. 10309-10335, 1986.

Baker, E.T. and G. J. Massoth. Hydrothermal Plume Measurements: A Regional Perspective. Science, vol. 234, pp. 980-982, 1986.

Baker, E. T. and G. J. Massoth. Characteristics of hydrothermal plumes from two vent fields on the Juan de Fuca Ridge, northeast Pacific Ocean. Earth and Planetary Science Letters, vol. 85, pp.59-73, 1987.

Bemis, K. G. and R. P. Von Herzen. Temperature profiles from the Juan de Fuca Ridge: heat flux from a simple plume model. EOS, vol.70 (43), p. 1327, 1989.

Campbell, I. H., T. J. McDougall, and J. S. Turner. A note on fluid dynamic processes which can influence the deposition of massive sulfides. Economic Geology, vol. 79, pp. 1905-1913, 1984.

Cann, J. R. and M. R. Strens. Black smokers fuelled by freezing magma. Nature, vol. 298, pp. 147-149, 1982.

Cann, J. R., M. R. Strens, and A. Rice. A simple magma-driven thermal balance model for the formation of volcanogenic massive sulphides. Earth and Planetary Science Letters, vol. 76. pp. 123 - 134, 1985.

Cannon, G. A. and D. J. Pashinski. Circulation near Axial Seamount. Journal of Geographical Research, vol. 95, pp. 12823-12828, 1990.

Cannon, G. A., D. J. Pashinski and M. R. Lemon. Mid-depth flow near hydrothermal venting sites on the Southern Juan de Fuca Ridge. Journal of Geographical Research, in press, 1991.

Chen, C. J. and W. Rodi. Vertical Turbulent Buoyant Jets: A Review of Experimental Data. Pergamon Press: New York, 1980.

Christeson, G. and G. M. Purdy. A seismic refraction experiment along the crest of the Northern Symmetrical Segment of the Juan de Fuca Ridge. EOS, vol. 70 (43), p. 1160, 1989.

Converse, D. R., H. D. Holland, and J. M. Edmond. Flow rates in the axial hot springs of the East Pacific Rise (21°N): implications for the heat budget and the formation of massive sulfide deposits. Earth and Planetary Science Letters, vol. 69, pp. 159-175, 1984.

Crane, K., F. Aikman III, R. Embley, S. Hammond, A. Malahoff, and J. Lupton. The distribution of geothermal fields on the Juan de Fuca Ridge. Journal of Geophysical Research, vol. 90, no. B1, pp. 727-744, 1985.

Csanady, G. T. Turbulent Diffusion in the Environment. D. Reidel Publishing Company: Boston, 1973.

Davis, E. E. and C. R. B. Lister. Fundamentals of ridge crest topography. Earth and Planetary Science Letters, vol.21, pp. 405-413,1974.

Delaney, J. R., V. Robigou, R. E. McDuff, and M. K. Tivey. A vigorous hydrothermal system: the Endeavor vent field, Northern Juan de Fuca Ridge. Submitted to Journal of Geophysical Research, 1991.

Embley, R. W., W. W. Chadwick, and C. G. Fox. New evidence for volcanic eruptions on the Southern Juan de Fuca Ridge during the 1980's - implications for megaplumes and seafloor monitoring. EOS, vol. 71, p.1602, 1990.

Fischer, H. B., E. J. List, R. C. Y. Koh, J. Imberger, and N. H. Brooks. Mixing in Inland and Coastal Waters. Academic Press: New York, 1979.

Fofonoff, N. P. and R. C. Millard Jr. Algorithms for computation of fundamental properties os seawater. Unesco Technical Papers in Marine Science, vol. 44, 1983.

Gerhart, P. M. and R. Gross. Fundamentals of Fluid Mechanics, chapter 8. Addison-Wesley Publishing Company, Inc., 1985.

Gifford, Jr., F. Statistical properties of a fluctuating plume dispersion model. Advances in Geophysics, vol. 6, pp. 117-137, 1959.

Gillis, K. M. and P. T. Robinson. Distribution of alteration zones in the upper oceanic crust. Geology, vol. 16, pp. 262-266, 1988.

Green, K. E., R. P. Von Herzen, and D. L. Williams. The Galapagos spreading center at 86°W: a detailed geothermal field study. Journal of Geophysical Research, vol. 86, pp. 979-986, 1981.

Kappel, E. S. and W. R. Normark. Morphometric variability within the axial zone of the Southern Juan de Fuca Ridge: interpretation from Sea MARC II, Sea MARC I, and deep-sea photography. Journal of Geophysical Research, vol. 92, pp. 11292-11302, 1987.

Karsten, J. L., J. R. Delaney, J. M. Rhodes and R. A. Lilas. Spatial and temporal evolution of magmatic systems beneath the Endeavor Segment, Juan de Fuca Ridge: tectonic and petrologic constraints. Journal of Geophysical Research, vol. 95, pp. 19235-19256, 1990.

Karsten, J. L., S. R. Hammond, E. E. Davis, and R. G. Currie. Detailed geomorphology and neotectonics of the Endeavor Segment, Juan de Fuca Ridge: new results from SeaBeam swath mapping. Geological Society of America Bulletin, vol. 97, pp. 213-221, 1986.

Kotsovinos, N. E. Temperature measurements in a turbulent round plume. International Journal of Heat and Mass Transfer, vol. 28, pp. 771-777, 1985.

Kotsovinos, N. E. and E. J. List. Plane turbulent buoyant jets. Part 1. Integral properties. Journal of Fluid Mechanics, vol. 81, pp. 25-44, 1977.

Kotsovinos, N. E. Plane turbulent buoyant jets. Part 2. Turbulence structure. Journal of Fluid Mechanics, vol. 81, pp. 45-62, 1977.

LaFlamme, B., J. R. Delaney, R. E. McDuff, V. Miller, V. Robigou, A. Schultz, M. Smith, J. Wells, J. Fondrik, and J. McClain. Observations and Experimental Studies in the Endeavor Hydrothermal Field _ Summer, 1988. EOS, vol. 70 (43), p. 1160, 1989.

Little, S.A., K. D. Stolzenbach, and R.P. Von Herzen. Measurements of plume flow from a hydrothermal vent field. Journal of Geophysical Research, vol. 92, no. B3, pages 2587-2596, 1987.

Lister, C. R. B. On the penetration of water into hot rock. Geophysical Journal of the Royal Astronomical Society, vol. 39, pp. 465-509, 1974.

Lister, C. R. B. The basic physics of water penetration into hot rock. Hydrothermal Processes at Seafloor Spreading Centers. Plenty Press: New York, pp. 141-168, 1983.

McConachy, T. F., R. D. Ballard, M. J. Mottl, R. P. Von Herzen. Geologic form and setting of a hydrothermal vent field at lat 10°56'N, East Pacific Rise: a detailed study using Angus and ALVIN. Geology, v. 14, p.295-298, 1986.

Macdonald, K. C. A geophysical comparison between fast and slow-spreading centers: constraints on magma chamber formation and hydrothermal activity. In: Hydrothermal Processes at Seafloor Spreading Centers, pp. 27-52. Eds. P. A. Rona, K. Boström, L. Laubier and K. L. Smith, Jr. Plenum Press: New York, 1983.

Macdonald, K. C., K. Becker, F. N. Spiess, and R.D. Ballard. Hydrothermal heat flux of the "black smoker" vents on the East Pacific Rise. Earth and Planetary Science Letters, 4:1-7, 1980.

Moran, J. E. and C. R. B. Lister. Heat flow across Cascadia Basin near 47°N, 128°W. Journal of Geophysical Research, vol. 92, pp.11416-11432, 1987.

Morton, B. R., Sir Geoffrey Taylor, F.R.S., J. S. Turner. Turbulent gravitational convection from maintained and instantaneous sources. Procedures of the Royal Society of London, Series A, vol. 234, pp. 1-23, 1956.

Morton, J. L. Oceanic spreading centers: Axial magma chambers, thermal structure, and small scale ridge jumps, Ph.D. thesis, Stanford University, Stanford, California, 1984.

Morton, J. L. and N. H. Sleep. A mid-oceanic ridge thermal model: constraints on the volume of axial hydrothermal heat flux. Journal of Geophysical Research, vol. 90, no. B13, pp. 11345-11353, 1985.

Mottl, M. J. Metabasalts, axial hot springs, and the structure of hydrothermal systems at mid-ocean ridges. Geological Society of America Bulletin, vol. 94, pp. 161-180, 1983.

Papanicolaou, P. N. and E. J. List. Statistical and spectral properties of tracer concentration in round buoyant jets. International Journal of Heat and Mass Transfer, vol. 30 (10), pp. 2059-2071, 1987.

Papanicolaou, P. N. and E. J. List. Investigations of round vertical turbulent buoyant jets. Journal of Fluid Mechanics, vol. 195, pp. 341-391, 1988.

Papantoniou, D. and E. J. List. Large-scale structure in the far field of buoyant jets. Journal of Fluid Mechanics, vol. 209, pp. 151-190, 1989.

Parker, R. L. and D. W. Oldenburg. Thermal models of ocean ridges, Nature, 242, pp. 137-139, 1973.

Parsons, B. and J. G. Sclater. An analysis of the variation of ocean floor bathymetry and heat flow with age. Journal of Geophysical Research, vol. 82, pp. 803-826, 1977.

Ricou, F. P. and D. B. Spalding. Measurements of entrainment by axisymmetrical turbulent jets. Journal of Fluid mechanics, vol. 11, p. 21-32, 1961.

Robigou, V., J. R. Delaney, R. E. McDuff, and M. K. Tivey. Geology of the Endeavor Segment of the Juan de Fuca Ridge and its associated hydrothermal fields. EOS, vol. 70 (43), p. 1161, 1989.

Rosenburg, N. D., J. E. Lupton, D. Kadko, R. Collier, M. D. Lilley, and H. Pak. Estimation of heat and chemical fluxes form a seafloor hydrothermal vent field using radon measurements. Nature, vol. 334, pp. 604-607, 1988.

Rouse, H., C. S. Yih, and H. W. Humphreys. Gravitational convection from a boundary source. Tellus, vol. 4, pp. 201-210, 1952.

Schouten, H., K. D. Klitgord, and J. A. Whitehead. Segmentation of mid-ocean ridges. Nature, vol. 317, pp. 325-329, 1985.

Schultz, A. Extended geophysical observations of ridge crest hydrothermal systems: heat flux and related quantities. EOS (abstract), vol. 71, p. 1619, 1990.

Shanks III, W. C. and W. E. Seyfried, Jr. Stable isotope studies of vent fluids and chimney materials, Southern Juan de Fuca Ridge: sodium metasomatism and seawater sulfate reduction. Journal of Geophysical Research, vol. 92, pp. 11387-11399, 1987.

Sleep, N. H. Hydrothermal convection at ridge axis. Hydrothermal Processes at Seafloor Spreading Centers. Plenty Press: New York, pp. 71-82, 1983.

Sleep, N. H. and T. J. Wolery. Egress of hot water from mid-ocean ridge hydrothermal systems: some thermal constraints. Journal of Geophysical Research, vol. 83 (B12), pp. 5913-5922, 1978.

Tennekes, H. and J. L. Lumley. A First Course in Turbulence. The MIT Press: Cambridge, 1972.

Tivey, M. K. and J. R. Delaney. Growth of large sulfide structures on the Endeavor Segment of the Juan de Fuca Ridge. Earth and Planetary Science Letters, vol. 77, pp. 303-317, 1986.

Thomsom, R. E., R. L. Gordon, and J. Dymond. Acoustic Doppler current profiler observations of a mid-ocean ridge hydrothermal plume. Journal of Geophysical Research, vol. 94, pp. 4709-4720, 1989.

Townsend, A. A., F. R. S. The Structure of Turbulent Shear Flow. Cambridge University Press: New York, 1976.

Turcotte, D. L. and G. Schubert. Geodynamics: Applications of Continuum Physics to Geological Problems. John Wiley and Sons: New York, 1982.

Turner, J. S. Buoyancy Effects in Fluids. Cambridge University Press: New York, 1973.

Weller, R. A., J. P. Dean, J. Marra, J. F. Price, E. A. Francis, and D. C. Boardman. Three-dimensional flow in the upper ocean, Science, vol. 227, pp. 1552-1556, 1985.

Wolery, T. J. and N. H. Sleep. Hydrothermal circulation and geochemical flux at mid-ocean ridges. The Journal of Geology, vol. 84, pp. 249-275, 1976.